

The Precipitation Response to an Idealized Subtropical Continent

ELIZABETH A. MAROON AND DARGAN M. W. FRIERSON

Department of Atmospheric Sciences, University of Washington, Seattle, Washington

SARAH M. KANG

School of Urban and Environmental Engineering, Ulsan National Institute of Science and Technology, Ulsan, South Korea

JACOB SCHEFF

Lamont-Doherty Earth Observatory, Columbia University, Palisades, New York

(Manuscript received 27 August 2015, in final form 11 February 2016)

ABSTRACT

A subtropical continent is added to two aquaplanet atmospheric general circulation models (AGCMs) to better understand the influence of land on tropical circulation and precipitation. The first model, the gray-radiation moist (GRaM) AGCM, has simplified physics, while the second model, the GFDL Atmospheric Model version 2.1 (AM2.1), is a fully comprehensive AGCM. Both models have a continent that is 60° wide in longitude from 10° to 30°N, in an otherwise slab-ocean-covered world. The precipitation response varies with cloudy- and clear-sky feedbacks and depends on continental albedo. In GRaM simulations with a continent, precipitation in the Northern Hemisphere decreases mostly as a result of decreased evaporation. In AM2.1 simulations, precipitation also shifts southward via Hadley circulation changes due to increasing albedo, but the radiative impact of clouds and moisture creates a more complex response. Results are similar when a seasonal cycle of insolation is included in AM2.1 simulations. The impact of a large, bright subtropical continent is to shift precipitation to the opposite hemisphere. In these simulations, the hemisphere of greater tropical precipitation is better predicted by the hemisphere with greater atmospheric energy input, as has been shown in previous literature, rather than the hemisphere that has higher surface temperature.

1. Introduction

The intertropical convergence zone (ITCZ) is associated with upward motion by the Hadley circulation and a maximum of zonal mean precipitation. The annual and zonal mean ITCZ is north of the equator, though its position is thought to have varied over the recent past (Hwang et al. 2013; Ridley et al. 2015) and the deeper past (Black et al. 1999; Haug et al. 2001; Koutavas and Lynch-Stieglitz 2003; Arbuszewski et al. 2013). Numerous model studies with hemispherically asymmetric forcings have noted accompanying ITCZ shifts (Rotstayn et al. 2000; Chiang et al. 2003; Chiang and Bitz 2005; Zhang and Delworth 2005; Broccoli et al. 2006; Yoshimori and

Broccoli 2008; L'Heveder et al. 2015; Kang et al. 2015a). It has been suggested that the northward cross-equatorial ocean heat transport by the Atlantic meridional overturning circulation is critical for displacing the ITCZ north of the equator in the present climate (Fučkar et al. 2013; Frierson et al. 2013; Marshall et al. 2013). In addition, Northern Hemisphere (NH) land is thought to be warmer than Southern Hemisphere (SH) land also owing to the role of northward ocean energy transport (Kang et al. 2015b).

There are two perspectives on what determines the ITCZ position. One perspective emphasizes surface temperature (e.g., Xie 2005; Cvijanovic and Chiang 2013). As surface pressure gradients in the tropics are determined by the surface temperature gradients, anomalous cross-equatorial boundary layer flows are driven by interhemispheric surface temperature gradients, and the ITCZ location is controlled by the region of convergence (Lindzen and Nigam 1987). The ITCZ

Corresponding author address: Elizabeth A. Maroon, Department of Atmospheric Sciences, University of Washington, Box 351640, Seattle, WA 98115.
E-mail: emaroon@uw.edu

position can also be interpreted as following the sea surface temperature (SST) maximum with threshold behavior near 28°C in the tropics (Gadgil et al. 1984; Zhang 1993; Sud et al. 1999).

The other perspective focuses on the atmospheric energy budget (e.g., Broccoli et al. 2006; Kang et al. 2008, 2009; Yoshimori and Broccoli 2009; Frierson and Hwang 2012; Seo et al. 2014; Maroon et al. 2015). An extratropical or tropical forcing that creates an inter-hemispheric gradient in energy can impact the Hadley circulation. As a result, the Hadley circulation transports energy across the equator in the direction of its upper branch and transports moisture across the equator the opposite direction by its lower branch, shifting the ITCZ to the hemisphere with greater energy. Since the Hadley circulation transports energy toward the cooler hemisphere, to partly compensate the cooling, the two perspectives are broadly consistent. Kang and Held (2012) argued that the atmospheric energy budget and the moist static stability determine the ITCZ response, not the surface temperature. The tropical surface temperature response is suggested to be a result of the surface energy budget and not a driver of the tropical precipitation response.

During the solstice seasons, much of the cross-equatorial surface flow in the Hadley circulation occurs in the Asian monsoon region (Dima and Wallace 2003). If the monsoon is thought of as the summer displacement of the ITCZ over land (Chao and Chen 2001; Gadgil 2003), then theories of the ITCZ can be applied to monsoon circulations. Lindzen and Hou (1988) showed off-equatorial heating resulted in a stronger (weaker) Hadley cell in the winter (summer) hemisphere, in the dry angular-momentum-conserving Held and Hou (1980) model. This variation in seasonal Hadley cell strength is also observed (Dima and Wallace 2003). The Hadley circulation has nonlinear threshold behavior in response to subtropical heating in this model (Plumb and Hou 1992), but outside this axisymmetric framework, this threshold behavior is not always present. In complex AGCMs, eddies are thought to play a large role in the formation of monsoon circulations (Privé and Plumb 2007a,b; Bordoni and Schneider 2008). Simulations with regional subtropical diabatic heating produce a Rossby and Kelvin wave response that affects dynamics outside the monsoon region (Gill 1980; Hoskins and Rodwell 1995). Rodwell and Hoskins (1996) connect diabatic heating from the summer Asian monsoon to the desertification of northern Africa, where NH summer subsidence from the Hadley circulation would otherwise be small.

Land surface effects also play a role in the subtropical precipitation distribution; Cook and Gnanadesikan (1991) show that the saturation of an idealized continent's

surface affects the precipitation distribution over the continent. Cook (2003) shows that the presence of continents in an AGCM simulation doubles the winter hemisphere Hadley cell's strength. Chou et al. (2001) note the importance of surface saturation on the precipitation of an idealized continent; they also show that ocean heat transport, ventilation, and the remote Rossby wave forcing of Rodwell and Hoskins (1996) all play a role in limiting the poleward extent of precipitation. Chou and Neelin (2001, 2003) both emphasize the importance of low moist static energy (MSE) air ventilation over the continent and show that the Sahara's high albedo limits the poleward extent of precipitation. Privé and Plumb (2007a,b) also examine the role of idealized continents in modifying the tropical circulation and precipitation; they show that a maximum in MSE predicts the poleward edge of the monsoon precipitation in their model, building on work by Emanuel et al. (1994). Karauskas and Ummenhofer (2014) show that the Hadley circulation is composed of distinct regional and opposing circulations associated with the distribution of continents.

Here, we build on these past studies and examine how a subtropical continent modifies the precipitation distribution, the tropical circulation, and the energetic budget as compared to an aquaplanet. One of our aims is to see how energy transport and SST are related to the precipitation distribution. The two should be broadly consistent. The divergence of the atmospheric energy transport is equal to the sum of the top-of-atmosphere (TOA) and surface energy budgets. SST is an important factor in setting the surface energy budget; SST is also important for the TOA heat budget but not in a straightforward way, owing to clouds. By adding subtropical land in our simulations, land surface temperature and column MSE are no longer as tightly linked because the land surface may be unsaturated. With limited surface moisture, surface-absorbed shortwave (SW) radiation must be balanced by increased sensible heat and longwave (LW) radiation surface fluxes, potentially raising land temperature. Ignoring cloud changes, increased clear-sky LW emission and greater reflected SW radiation could decrease column MSE while simultaneously having a higher surface temperature. Should zonal mean precipitation then move toward the hotter, but drier, hemisphere? If the hot continent is a net energy sink, then the temperature and energetic perspectives will have predicted different locations.

We also explore a result from Frierson et al. (2013): the net TOA radiative imbalance (ignoring ocean heat transport) would indicate greater SH precipitation; the largest contributor to this TOA imbalance is from the Sahara. To test this hypothesis, our idealized continent is

loosely based on the approximate size and shape of the Sahara, and we also examine the role of continental albedo.

The two AGCMs used are described in [section 2](#). [Section 3](#) contains the results for the simpler model, while [section 4](#) contains results for the more comprehensive AGCM. The seasonal cycle's impact in the comprehensive model is discussed in [section 5](#), with conclusions in [section 6](#).

2. Models

Two GFDL AGCMs, the gray-radiation moist (GRaM) AGCM and the Atmospheric Model version 2.1 (AM2.1), coupled to a mixed layer ocean, are used in this study. This version of GRaM ([Frierson et al. 2006](#)) has a B-grid core with $2^\circ \times 2^\circ$ resolution and 25 vertical levels. The model includes latent heat release by condensation, but with gray radiation, water vapor does not impact radiation. Insolation is set to approximate the annual mean, and SW absorption in the atmospheric column is set to 0.2; there is no seasonal or diurnal cycle and there is no sea ice. Because there are no clouds, the albedo is set to 0.29 over the ocean to bring the atmospheric energy budget closer to observed. LW radiation is calculated in one band with a prescribed optical depth meant to mimic the impact of water vapor. There are no cloud, ice, or water vapor radiative feedbacks in either the SW or LW radiation. Large-scale condensation along with a simplified Betts–Miller convection scheme ([Frierson 2007](#)) is used.

An aquaplanet version of the GFDL AM2.1 with a mixed layer ocean is used with annual mean insolation ([Anderson et al. 2004](#); [Delworth et al. 2006](#); [Kang et al. 2008](#)). All fields that would produce an asymmetric radiative forcing (e.g., ozone) have been symmetrized about the equator, and as with GRaM, there is no sea ice. The dynamical core uses finite-volume numerics with $2.5^\circ \times 2^\circ$ horizontal resolution and 24 vertical hybrid pressure–sigma levels. The model has more elaborate physics than GRaM; comprehensive radiation, convection, and cloud schemes are implemented, and cloud and water vapor feedbacks are present. The radiative impact of aerosols is not included. A relaxed Arakawa–Schubert scheme ([Moorthi and Suarez 1992](#)) is used. The heat capacity of the slab ocean in both models is $1 \times 10^7 \text{ JK}^{-1} \text{ m}^{-2}$ (which corresponds to 2.4 m of water). The shallow mixed layer depth decreases the integration time to equilibrium and has little effect on the mean climate in comparison to deeper mixed layers in simulations without a seasonal cycle ([Kang et al. 2008](#)).

The effect of the seasonal cycle on precipitation location is also tested in a set of AM2.1 simulations; for

these experiments, the mixed layer heat capacity is increased to $1 \times 10^8 \text{ JK}^{-1} \text{ m}^{-2}$ (24 m of water) and no surface heat flux was used. These simulations address how robust the precipitation response is to seasonally varying insolation. We do not address the effect of seasonal cycle in the GRaM simulations as our version of this model does not yet have a seasonal cycle implemented.

A single NH continent, inspired by the Sahara, is placed in the subtropics. The continent has its southern and northern boundaries at 10° and 30°N and its western and eastern boundaries at 120° and 180° longitude. Aquaplanet simulations in both models were completed for comparison to the single continent simulations.

Both models were coupled to the GFDL Land Model version 2 (LM2). This configuration of GRaM uses LM2.0 ([Milly and Shmakin 2002](#)), and this configuration of AM2.1 uses the similar LM2.1 ([Delworth et al. 2006](#)). Our specific AM2.1 configuration allows land location to be varied and was first implemented by [Shi and Durran \(2014\)](#). LM2 hydrology is a simple one-bucket model, only a few steps more advanced from [Manabe \(1969\)](#). When the soil water reservoir reaches its maximum capacity, excess water runs off. Evapotranspiration is directly limited by soil moisture. Land parameters in both GRaM and AM2.1 are constant in time and space. In GRaM, the parameters used are the defaults for the Intermediate Complexity Climate Model (ICCMp1; [Farneti and Vallis 2009](#)), from which our land-configurable version of GRaM was derived. These idealized values were likely chosen to cool off land in ICCMp1 that is too hot. The soil thermal diffusivity is six orders of magnitude too large, but the heat capacity of the land is very small in GRaM, and we are not conducting any simulations in GRaM with a seasonal or diurnal cycle. In AM2.1, the default land parameters are those from [Scheff \(2014\)](#); for vegetation, these parameters represent mixed broadleaf/needleleaf trees for all but the roughness, which is more representative of grassland. [Table 1](#) compares the default parameters; in some cases they are very different.

In GRaM, land albedos of 0.15, 0.29, 0.40, and 0.60 are used, while in AM2.1, albedos of 0.0, 0.06, 0.20, 0.30, 0.40, and 0.60 are used; these albedos are chosen to span a wide range of possible albedos. From these two sets of experiments, a “dark” and a “light” simulation from each model are chosen for key comparison. As the default ocean albedo in GRaM is 0.29 (because GRaM has no clouds), the GRaM simulation with the land albedo of 0.29 is referred to as the dark GRaM case. We compare this dark simulation with the aquaplanet simulation and a light continent simulation with a land albedo of 0.40. The AM2.1 simulation with 0.06 land albedo is the dark AM2.1 simulation since 0.06 is similar

TABLE 1. Land model parameters used in GRaM and AM2.1 simulations.

Parameter	AM2.1	GRaM
Soil bucket capacity (mm)	162	208
Momentum roughness length (m)	0.07	0.01
Scalar roughness length (m)	0.0095	0.0014
Well-watered bulk stomatal resistance (s m^{-1})	17.4	0.01
Soil heat capacity in upper layers ($\text{J K}^{-1} \text{m}^{-3}$)	5.25×10^5	1.0×10^5
Soil heat capacity in lower layers ($\text{J K}^{-1} \text{m}^{-3}$)	2.1×10^6	1.0×10^5
Soil thermal diffusivity ($\text{m}^2 \text{s}^{-1}$)	5.8×10^{-7}	1.0

to the ocean's albedo near the continent (the ocean albedo varies with zenith angle). The dark AM2.1 simulation is compared with the aquaplanet simulation and a light simulation with a desertlike land albedo of 0.30. For comparison, the albedo of the Sahara is 0.30–0.40 (Ba et al. 2001). Seasonal cycle simulations in AM2.1 were completed with the same dark and light land albedos as in the annual mean simulations.

Annual mean GRaM and AM2.1 simulations are spun up for 10 years, with an additional 5 years of simulation for the climatology. For the AM2.1 simulations with seasons, the model was initialized from the annual mean

simulation with corresponding geometry and land albedo and spun up for 20 years; the climatology is constructed from an additional 20 years beyond the spinup period.

The climatologies of both models as aquaplanets have a few notable differences (Fig. 1). The ITCZ in the GRaM simulation has a smaller precipitation maximum and is wider than the ITCZ in the AM2.1 simulation. The subtropics in the AM2.1 simulation are drier than in the GRaM simulation. The GRaM simulation also has a weaker Hadley circulation, weaker jets, and a lower tropopause when compared with those of AM2.1.

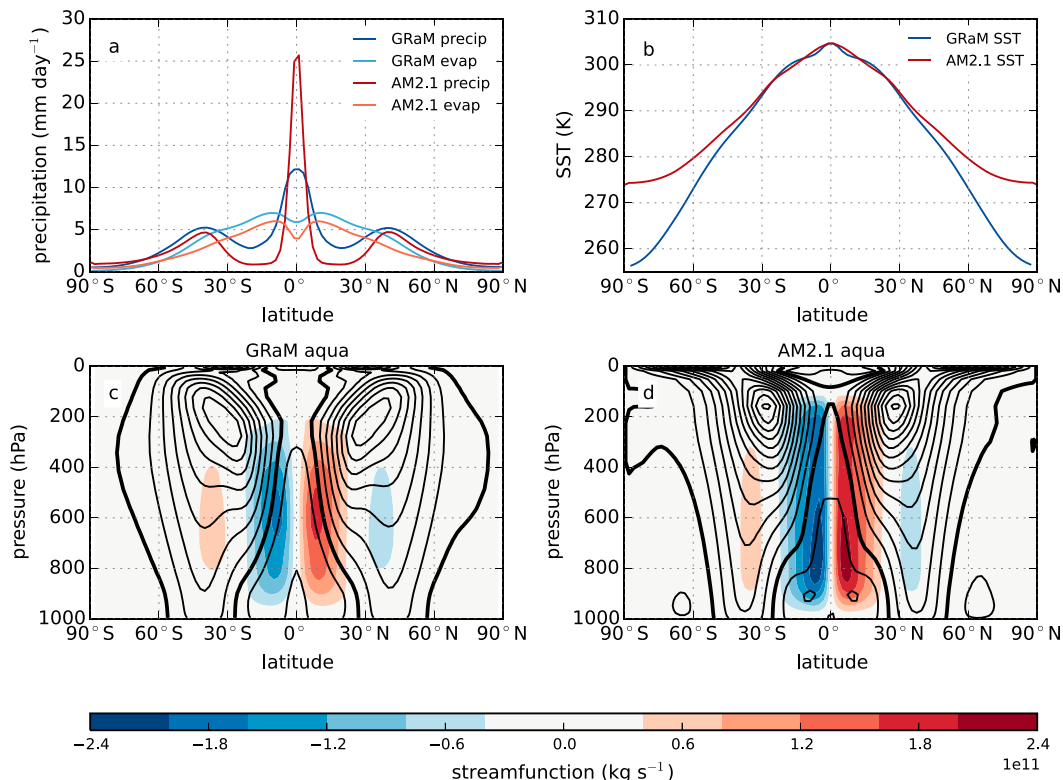


FIG. 1. Zonal mean climatologies for the aquaplanet GRaM and AM2.1 simulations. (a) Zonal mean precipitation and evaporation and (b) SST. The zonal-mean zonal wind (black contours) and overturning streamfunction (shading) are shown for both the (c) GRaM and (d) AM2.1 aquaplanet simulations. Wind contours are spaced every 5 m s^{-1} with the westerly wind in solid contours, easterly wind in dashed contours, and the zero wind as a solid thick contour. Red (blue) streamfunction is clockwise (counterclockwise).

3. The response of precipitation in GRaM simulations

To understand the impact of a subtropical continent on tropical precipitation in the simplest context, we start with a GRaM simulation that has a continent with the same albedo as the ocean. Later, we vary the continental albedo as well.

a. Dark continent simulation

Compared to the aquaplanet GRaM simulation, the addition of a continent with the ocean's albedo decreases precipitation over the continent and over the ocean directly south of the continent (Figs. 2a,c). Much of the precipitation decrease over the continent is due to a decrease in evaporation (Fig. 2c). Zonal mean evaporation decreases by about 0.7 mm day^{-1} , owing to the decrease of about 4 mm day^{-1} over the continent. Evaporation decreases by more than 90% over more of the continent; adding a dry continent significantly decreases evaporation, as would be expected.

Moisture convergence by mean meridional circulation (MMC) changes with the addition of the continent (Fig. 2d). We calculate the changes in MMC moisture convergence as follows:

$$-\nabla \cdot \int \frac{\delta[\bar{v}][\bar{q}]}{g} dp = -\nabla \cdot \int \frac{\{\bar{v}\}\delta[\bar{q}]}{g} dp - \nabla \cdot \int \frac{\{\bar{q}\}\delta[\bar{v}]}{g} dp, \quad (1)$$

where v is the meridional wind component, q is the specific humidity, g is the gravitational acceleration, square brackets $[\cdot]$ are zonal means, overbars are time means, δ refers to the difference in the quantity between two simulations (e.g., $v_{\text{cont}} - v_{\text{aquaplanet}}$), and the curly brackets $\{\cdot\}$ refer to the mean of a quantity in those two simulations [e.g., $(v_{\text{cont}} + v_{\text{aquaplanet}})/2$]. Here, ∇ represents the horizontal spherical divergence operator; because the quantities are already zonally averaged, the divergence is equivalent to the latitude ϕ component of the divergence $\{a \cos(\phi)\}^{-1} \partial \{\cos(\phi) A_\phi\} / \partial \phi$, where A_ϕ is the quantity that being operating on and a is Earth's radius. The vertical integrals are calculated over the entire column; for a full derivation of the water vapor budget and spherical divergence, see Peixoto and Oort (1992).

In the dark continent simulation, the decreased moisture convergence to the south of the continent is more due to changes in circulation (Fig. 2d, dark green line) than changes in moisture (Fig. 2d, dark purple line). The overturning circulation weakens in the NH because of the continent (Fig. 2e). This circulation change

between 0° and 15°N extends through the troposphere and has anomalous ascent over the southern portion of the continent, while subsidence at 30°N is enhanced. At the surface, the weakened overturning circulation decreases moisture convergence on the northern side of the ITCZ, decreasing ITCZ precipitation (Figs. 2e and 3a). Over the southern half of the continent, the anomalous moisture convergence offsets some of the decreased evaporation.

The soil is not saturated, disfavoring evaporation. As a result, the absorbed surface SW radiation is now balanced by increases in sensible heat flux and upward LW flux over the continent, and the surface temperature increases (Figs. 2a and 3a). The NH temperature is higher than that of the SH (Fig. 4a, dark blue line). If hemispheric precipitation were solely dependent on surface temperature, then the hotter NH would have greater precipitation than the SH. However, the decrease in evaporation due to a lack of surface moisture disfavors greater NH precipitation. The interhemispheric difference in total (combined land and ocean) surface temperature therefore predicts the wrong hemisphere for greater precipitation. The interhemispheric difference of SST (which does not include the unsaturated surface) could be a better measure of which hemisphere has greater precipitation because it only includes regions where boundary layer moisture is available. However, in this simulation, the NH also has higher SST because of the continent's proximity (Figs. 2a and 3a). Compared to the SH, the NH has higher SST in the tropics (Fig. 4b, dark blue line). Precipitation decreases near the continent, even though SST is higher than at the equator (Fig. 3a). The change in the land-induced circulation and stability is more important for determining precipitation than is the local SST.

Although the change in mass transport at the equator is small, there is a small heat transport from the SH to the NH. This must be balanced by an interhemispheric difference in the net TOA radiation budget (e.g., Kang et al. 2008). The NH-SH difference in net TOA radiation is negative (Fig. 4c, dark blue line) because of increased OLR over the northern half of the continent due to its higher temperature (there are no greenhouse or cloud radiative effects in GRaM). The NH has a net sink of MSE compared to the SH, so there is energy flux into that hemisphere. Regardless, in this simulation, the precipitation changes are mostly due to evaporation. In Kang et al. (2009), which connects changes in precipitation to the energetic budget, changes in evaporation are assumed to be small; here, the addition of a dry continent results in a large evaporation change relative to the aquaplanet.

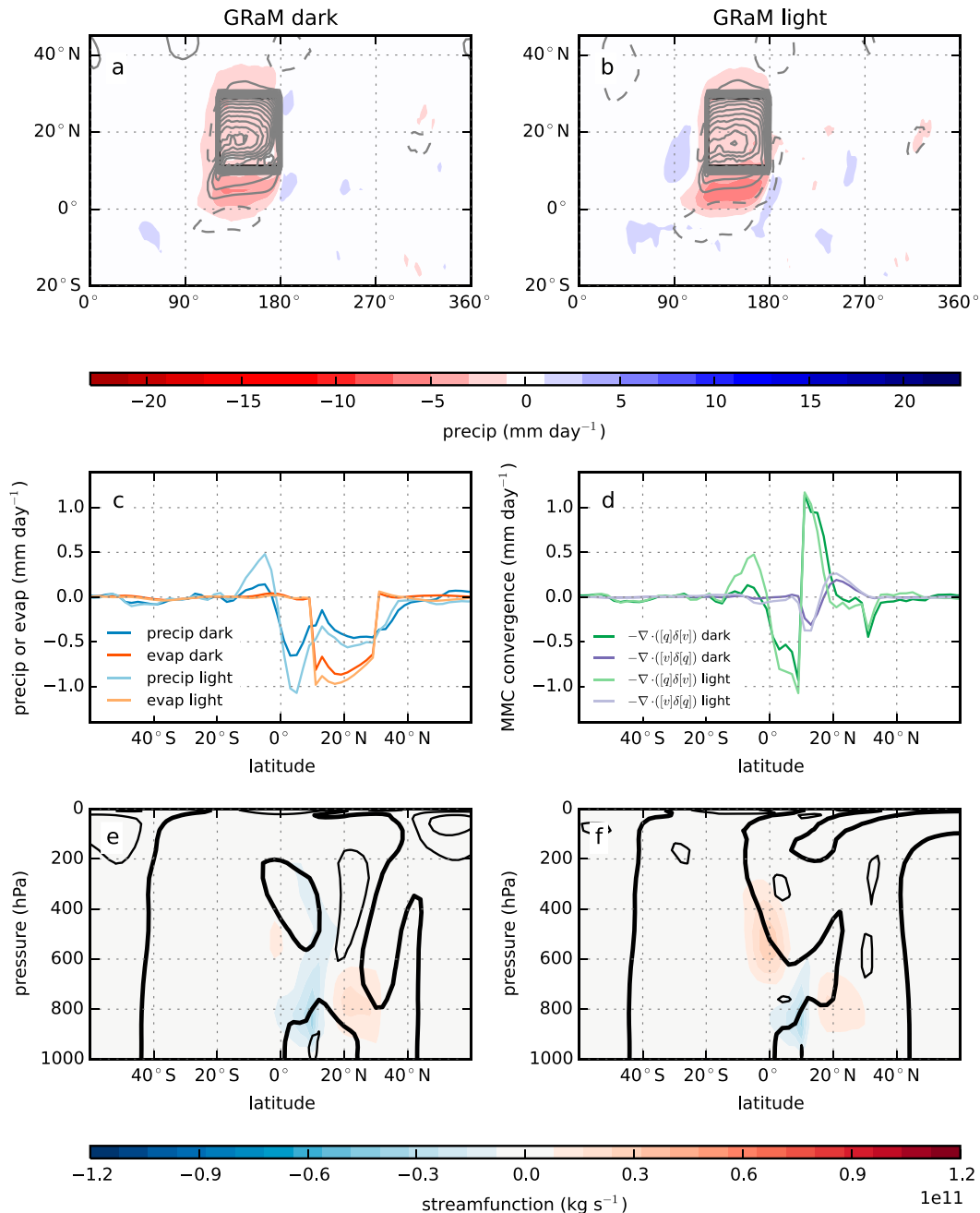


FIG. 2. Change in dark and light GRaM simulations from an aquaplanet. Shown are changes in precipitation (shading) and surface temperature (contours) from an aquaplanet in the (a) dark and (b) light simulations. Solid (dashed) contours indicate a positive (negative) surface temperature change; the contours start at ± 0.5 K, with a contour interval of 1 K, and the zero contour is omitted. (c) Zonal mean change in precipitation (blue) and evaporation (orange) from adding a continent. (d) Change in the mean meridional circulation component of moisture convergence due to changes in circulation (green) and moisture (purple). The quantities for the dark (light) continent simulations are in the darker (lighter) shades of the colors. Also shown are changes in streamfunction (shading) and zonal wind (contours) for the (e) dark and (f) light continent simulations. Zonal wind is contoured every 1 m s^{-1} and the zero zonal wind contour is thickened, positive contours are solid, and negative contours are dashed.

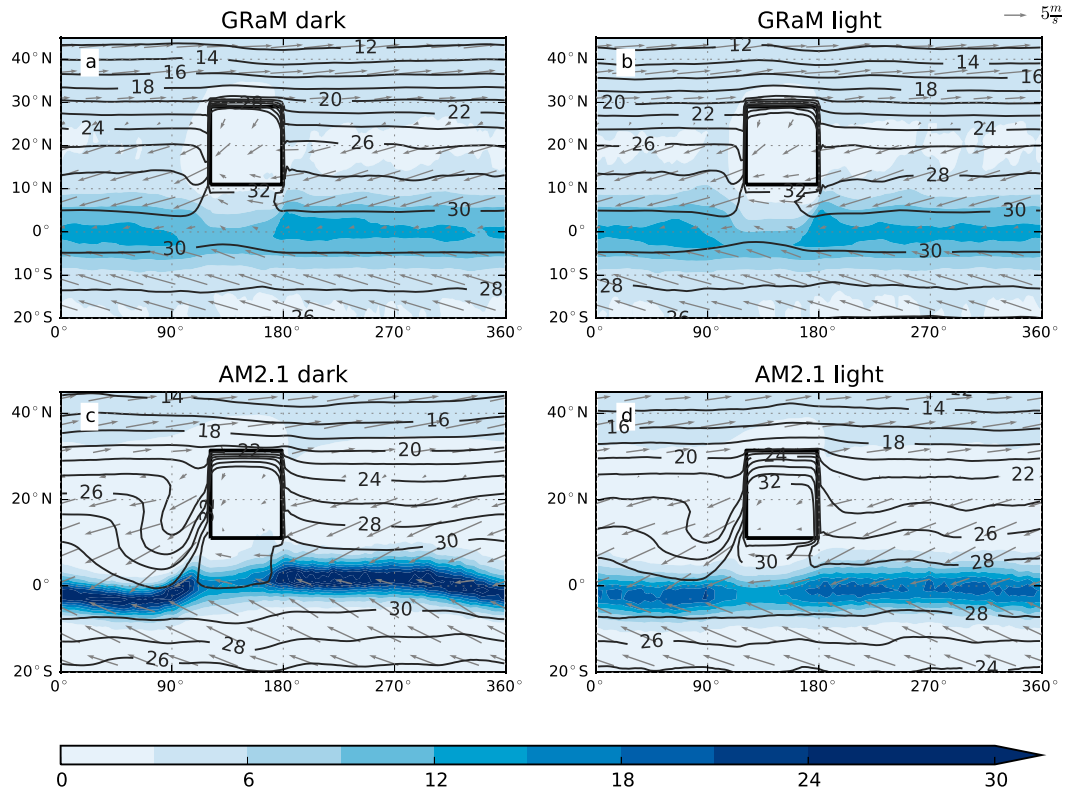


FIG. 3. Precipitation (mm day^{-1} ; shading), surface temperature ($^{\circ}\text{C}$; contours), and 10-m wind (arrows) in dark and light (a),(b) GRaM and (c),(d) AM2.1 simulations.

b. Continents with varying albedo

With a higher-albedo continent, precipitation decreases similarly to the dark continent simulation (Fig. 2b). However, the ITCZ shifts more noticeably to the south (Fig. 2c, light blue line). The evaporation decrease over the continent is still large (Fig. 2c, light red line), but there is also anomalous moisture convergence south of the equator due to small changes in the MMC (Fig. 2d, light green line). In the upper troposphere, there is an anomalous cross-equatorial Hadley circulation (Fig. 2f). This feature was weaker in the dark simulation (Fig. 2e). This anomalous circulation transports MSE from the SH to NH and transports moisture southward between 800 and 600 hPa at the equator (Fig. 2d, light green line). At the surface, the anomalous land-induced circulation decreases the southward moisture transport into the ITCZ (Fig. 5). With higher albedo, the southward moisture transport in the 800–600-hPa layer becomes larger than the northward surface transport.

In this simulation, precipitation is still mostly constrained by evaporation, but a small amount of the ITCZ shift can be attributed to the interhemispheric difference in TOA radiation (Fig. 2c, light blue line). The SSTs are larger in the NH tropics than in the SH tropics (Figs. 2b,

3b, and 4b), as they were in the dark simulation. Over the entire hemisphere, SST are slightly lower in the NH than in the SH, mainly from a SST decrease in the northern extratropics. These decreased SSTs are accompanied by a weak decrease in OLR in the NH extratropics (Fig. 4c, light blue line) and are due to decreased NH heat transport. However, the largest change in the hemispheric difference of TOA net radiation comes from the decreased SW flux from higher land albedo.

The NH–SH difference in net TOA radiation is proportional to the transport of energy across the equator. Greater energy in the SH compared to the NH indicates a northward transport of energy. This northward transport of energy would accompany a southward shift of precipitation minus evaporation ($P - E$) along the equator if the Hadley circulation changes there. Examining $P - E$ accounts for evaporation and shows how much of the moisture transport change can be attributed to the energy budget. Figure 6a shows the NH–SH difference in TOA net radiation against NH–SH difference in $P - E$, and Figs. 6b,c break this quantity into NH–SH differences in TOA LW and SW radiation (both defined as positive for an addition of energy into the atmosphere). With increasing albedo, the NH–SH difference in SW radiation becomes more negative because of

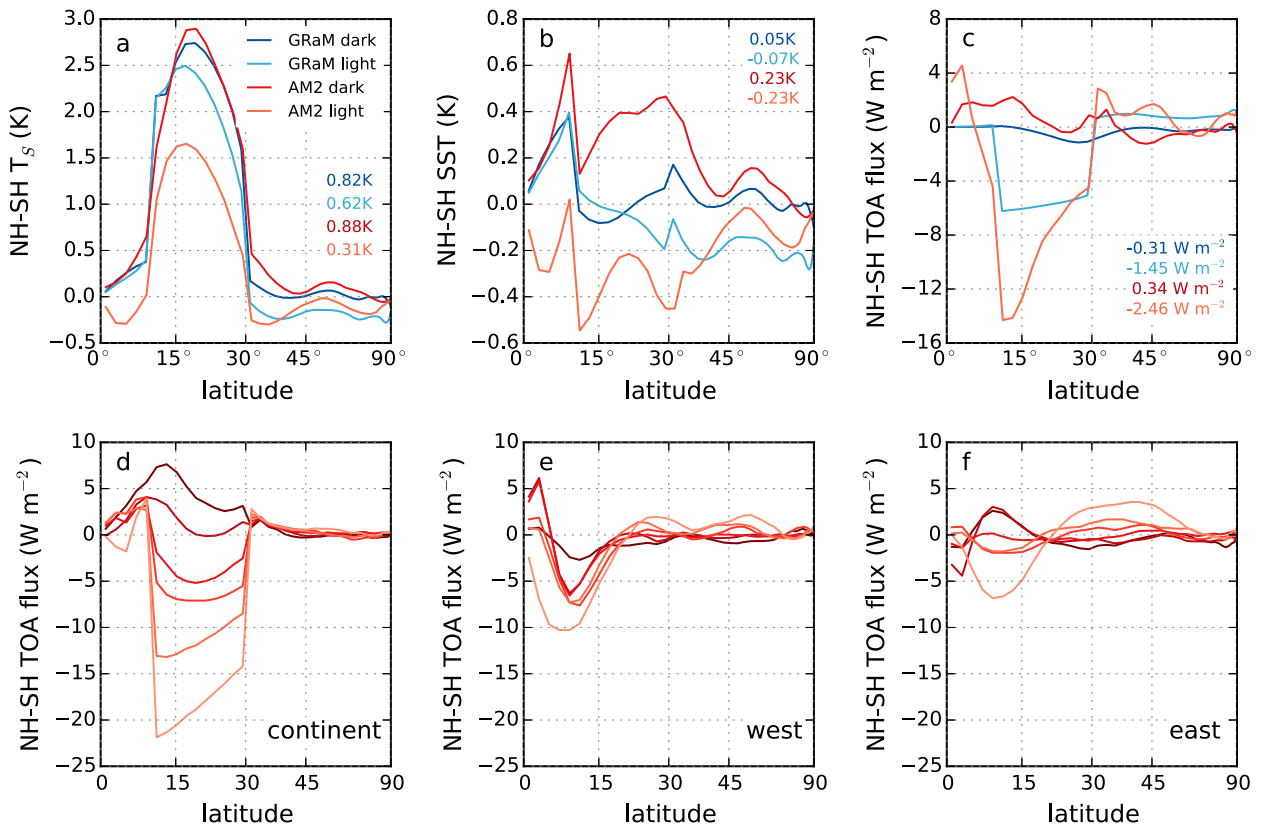


FIG. 4. NH minus SH plots for dark and light albedo rectangular continents in GRaM and AM2.1 simulations. (a) Surface temperature, (b) SST, and (c) TOA net radiation are shown for the GRaM (blue) and AM2.1 (red) continent simulations. In (a)–(c), the darker (lighter) colors refer to the dark (light) albedo simulation. The values shown are the area-weighted average of the hemispheric difference (NH minus SH) for the quantity in that panel; font colors correspond to the same colors as the line for each simulation. (d)–(f) Different zonal portions of the NH–SH difference in TOA net radiation for the AM2.1 simulations with different land albedos. The darker the shade of the red line, the darker the albedo of that simulation. Shown in (d) is the portion of the TOA radiation budget between 120° and 180° longitude where the continent is located. Shown in (e) [(f)] is the portion of the budget to the west (east) of the continent from 330° to 120° (from 180° to 330°) longitude. The lines in (d)–(f) are weighted such that directly taking the mean of the three lines for one simulation would yield the mean hemispheric difference in TOA radiation. Note that area-weighted latitude is used here.

increasing NH reflection, the NH–SH difference in LW radiation increases with increasing albedo as a result of decreasing OLR from the lower surface temperatures. For a given albedo, the NH–SH difference in LW radiation partially offsets the NH–SH SW radiation changes, leading to an NH–SH net radiation change that has the same sign as SW radiation. The NH–SH $P - E$ difference is linear with changes in all three NH–SH differences in radiation quantities. The amount of hemispheric precipitation asymmetry that is not due to evaporation can be attributed to circulation changes at the equator.

4. The response of precipitation in AM2.1 simulations

Equivalent simulations are completed in the AM2.1 model for comparison to the GRaM simulations. The land albedo in the dark AM2.1 simulation is 0.06 (the

approximate albedo of the subtropical ocean), while the albedo in the light AM2.1 simulation is 0.30. The AM2.1 simulations with a subtropical continent have a more complex response than the GRaM simulations because of the radiative impact of clouds and water vapor feedbacks.

a. Dark continent simulation

Subtropical precipitation in the AM2.1 aquaplanet model is already low (Fig. 1a), so the addition of a continent can decrease precipitation by only a small amount over the continent (Fig. 7a). The change in evaporation over the continent in the AM2.1 simulation is similar to the evaporation change in GRaM (note different y-axis scales between Figs. 2c and 7c). In contrast to evaporation, the change in the tropical precipitation in AM2.1 is much larger than in GRaM and is due to larger relative changes in moisture convergence.

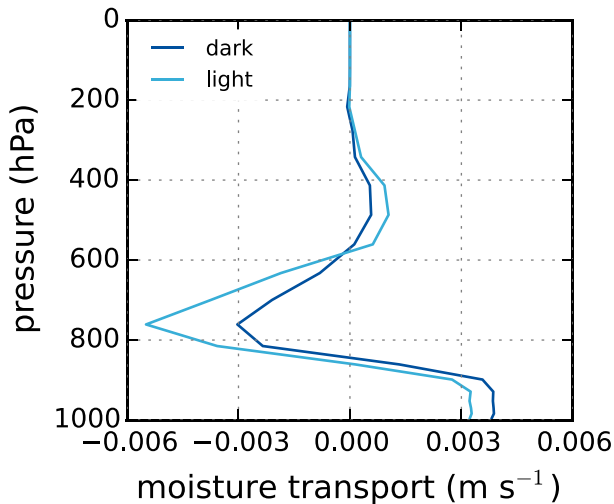


FIG. 5. Change in moisture transport across the equator by the MMC ($\overline{v}|\overline{q}$) with height due to meridional wind changes in GRaM continent simulations compared to an aquaplanet simulation. The dark blue line is for the dark albedo simulation, and the light blue line is for the light albedo simulation.

As in the light GRaM simulation, these changes are mostly due to changes in the MMC, not to changes in moisture (Fig. 7d). Changes in the MMC moisture transport are larger than the changes in precipitation due to transients. Also unlike the GRaM simulations, in the AM2.1 dark simulation, there is large zonal variation in precipitation and vertical motion (Figs. 7a and 8). To the west of the continent, the ascending motion shifts southward and precipitation moves south with it; to the east of the continent, the opposite happens. In the zonal band with the continent, a shallow land-induced circulation develops with ascending air over the southern half of the continent (Fig. 8b). There is also deep anomalous descent at the equator in this region. A northward shift of the NH jet also occurs as a result of the addition of the dark continent (Fig. 7e). The shift is strongest at 200 hPa, occurs at all longitudes, and also appears weakly at the surface. This jet shift could be associated with changes in baroclinicity associated with meridional surface temperature gradient changes, resulting from changes in cloud cover or latent heating due to the different surface type.

In the deep tropics, these regional precipitation shifts sum to a zonal mean precipitation decrease at the equator and an increase on its flanks (Fig. 7c), coincident with a decrease in the strength of the Hadley circulation (Fig. 7e). Part of the explanation for these sharp precipitation shifts is that the ITCZ in the AM2.1 control simulation is already very narrow (Fig. 1a); a small displacement of the ITCZ leads to a large change in local precipitation.

In this simulation, there is slightly greater precipitation in the NH. As examined previously with the GRaM simulations, we look at whether the precipitation follows the warmer hemisphere or the hemisphere with greater energy. Overall, the total surface temperature and SST are higher in the NH, though temperature changes are not spatially uniform. In the region of the continent, SST increases north of the equator, up to 32°C, while precipitation decreases at the equator (Figs. 3c and 7a). The hottest SSTs in the deep tropics are associated with a region of decreased precipitation because the tropical circulation is less amenable to deep convection. Other regions show notable changes in SST. Anomalously low SSTs form to the west of the continent because of increasing low clouds. The NH is also the hemisphere with more absorbed radiation. In this simulation, there is higher hemispheric-average SST and TOA net radiation in the hemisphere of greater precipitation (Figs. 4a–c, dark red lines). As a result, this simulation cannot distinguish between the SST and energetic perspectives on the hemisphere of greater precipitation, as both perspectives would predict the NH hemisphere. However, the local relation between SST and precipitation is not consistent; the region with highest SST does not have the greatest precipitation (Fig. 3c).

Because of the zonally varying ITCZ shifts, the hemispheric difference in TOA net radiation is composed of zonally compensating terms. Figures 9 and 10 decompose the TOA radiation budget into LW and SW clear- and cloudy-sky terms. To diagnose LW radiation changes, the TOA LW radiation is decomposed into the clear-sky LW component (which is a model diagnostic) and LW cloud forcing (the difference of the total and the clear sky). The SW cloudy and clear sky portions are calculated using the approximate partial radiative perturbation (APRP) method (Taylor et al. 2007), which takes cloud masking into account. Using the APRP method, changes in SW radiative forcing are decomposed into the changes due to cloud fraction, atmospheric scattering coefficient in clear and cloudy conditions, surface albedo in clear and overcast skies, and clear-sky and cloud absorption; a positive sign indicates energy into the atmosphere. Here, we use the changes in the terms from cloud fraction and cloud scattering for the change in SW cloud radiation. The remainder of the terms, surface albedo in clear-sky and overcast conditions, clear-sky atmospheric scattering, and clear-sky atmospheric absorption, constitute the change in SW clear-sky radiation. The residual term in the APRP decomposition is small.

In the dark simulation, the NH absorbs slightly more energy than the SH (Fig. 9a, black line). Having greater

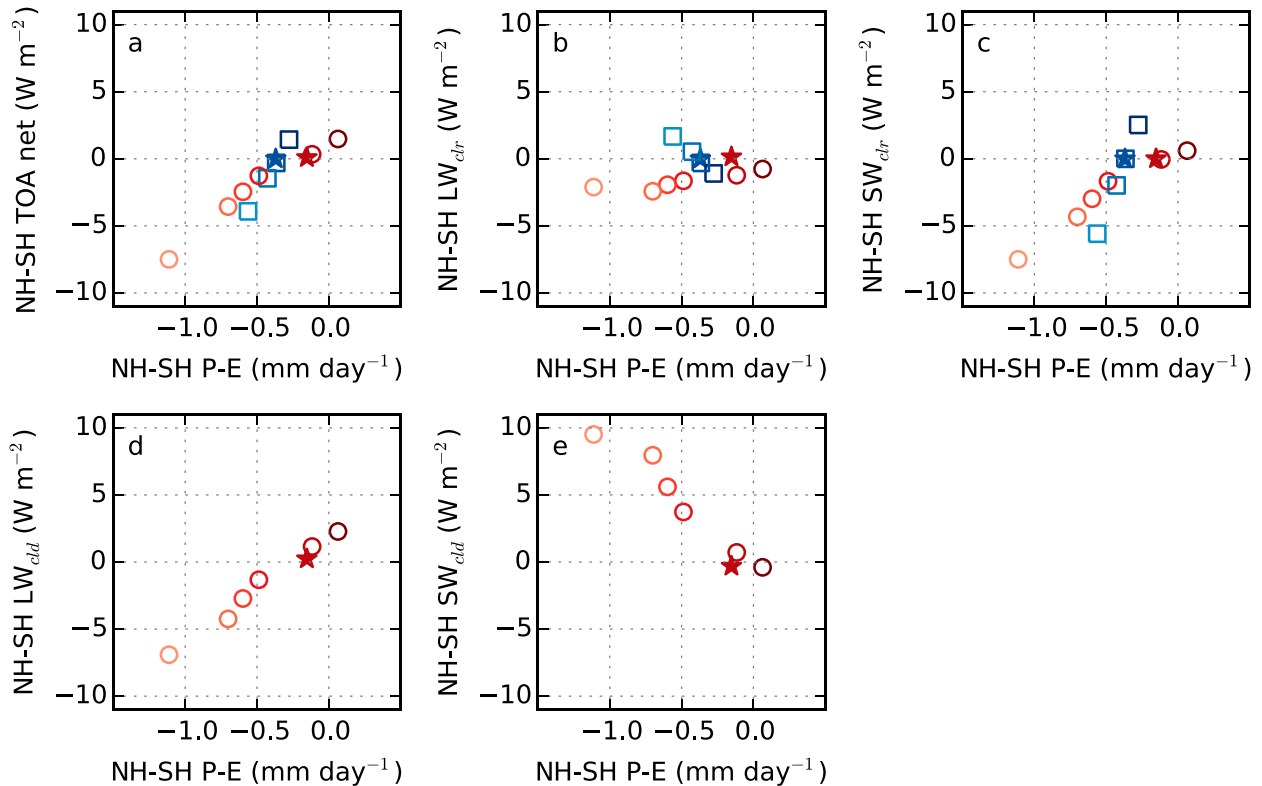


FIG. 6. (a) NH minus SH tropical $P - E$ and NH minus SH radiative imbalance for GRaM and AM2.1 continent simulations. The NH-SH tropical $P - E$ difference is defined here as the difference of area-weighted mean $P - E$ from 0° to 90°N and 0° to 90°S . The NH-SH difference in TOA radiation is decomposed into (b) LW clear-sky radiation, (c) SW clear-sky radiation, (d) LW cloudy-sky radiation, and (e) SW cloudy-sky radiation. Blue squares are rectangular-continent GRaM simulations, while red circles are rectangular-continent AM2.1 simulations. The darker the color of the marker, the lower the land albedo is. The blue (red) star is the GRaM (AM2.1) aquaplanet simulation. TOA SW and LW radiation are defined to be positive when they add energy to the planet.

net energy input in the NH would favor greater precipitation in the NH as well, as described above. Though the NH absorbs slightly more energy than the SH, the longitudinal variation in the individual radiation terms is large because of the varying directions of ITCZ shifts and the direct impact of the continent. Where the ITCZ shifts across the equator, changes in LW and SW cloud radiation oppose each other. When the ITCZ clouds shift toward one hemisphere, the deep clouds reduce SW radiation absorbed there, but they also cause greater LW trapping (Figs. 10a,e). The opposite happens when the ITCZ clouds shifts away; there is more absorbed SW radiation because of decreased reflection by deep clouds, and there is more OLR with fewer high clouds. In the deep tropics, the changes in SW cloud radiation are larger than those from LW cloud radiation. The combined SW and LW cloud radiative changes oppose the shift in the ITCZ because they decrease the net energy into the hemisphere with the ITCZ (Figs. 10a,e). ITCZ shifts also change the clear-sky LW radiation absorbed in the deep tropics; with greater moisture in the shifted ITCZ, more clear-sky LW radiation is

trapped (Fig. 10g). Where the ITCZ shifts, the SW term dominates over LW cloudy and clear sky together. In the zonal mean, the changes in clear-sky LW forcing are small equatorward of 5° (Fig. 9a). SW cloud radiation changes dominate because of the positive NH SW cloud radiation changes in the longitudes of the continent (Fig. 10a). From 5° to 15° latitude, LW clear- and cloudy-sky forcing is larger than SW forcing. As a result, NH-SH difference in TOA net radiation is positive, indicating greater energy input into the NH, which is also where the zonal mean precipitation has shifted.

There are other notable radiation changes associated with the addition of the continent. In this AM2.1 simulation, these other changes altogether have a small net impact on the interhemispheric difference in TOA radiation. Decreases in low clouds over the continent lead to more absorbed SW radiation, especially over its northwestern corner (Fig. 10a). Low stratus clouds form west of the continent, which decreases the absorbed SW radiation. The formation of these clouds could be due to dry continental air temporarily increasing evaporation, cooling the surface, and increasing subsidence. This

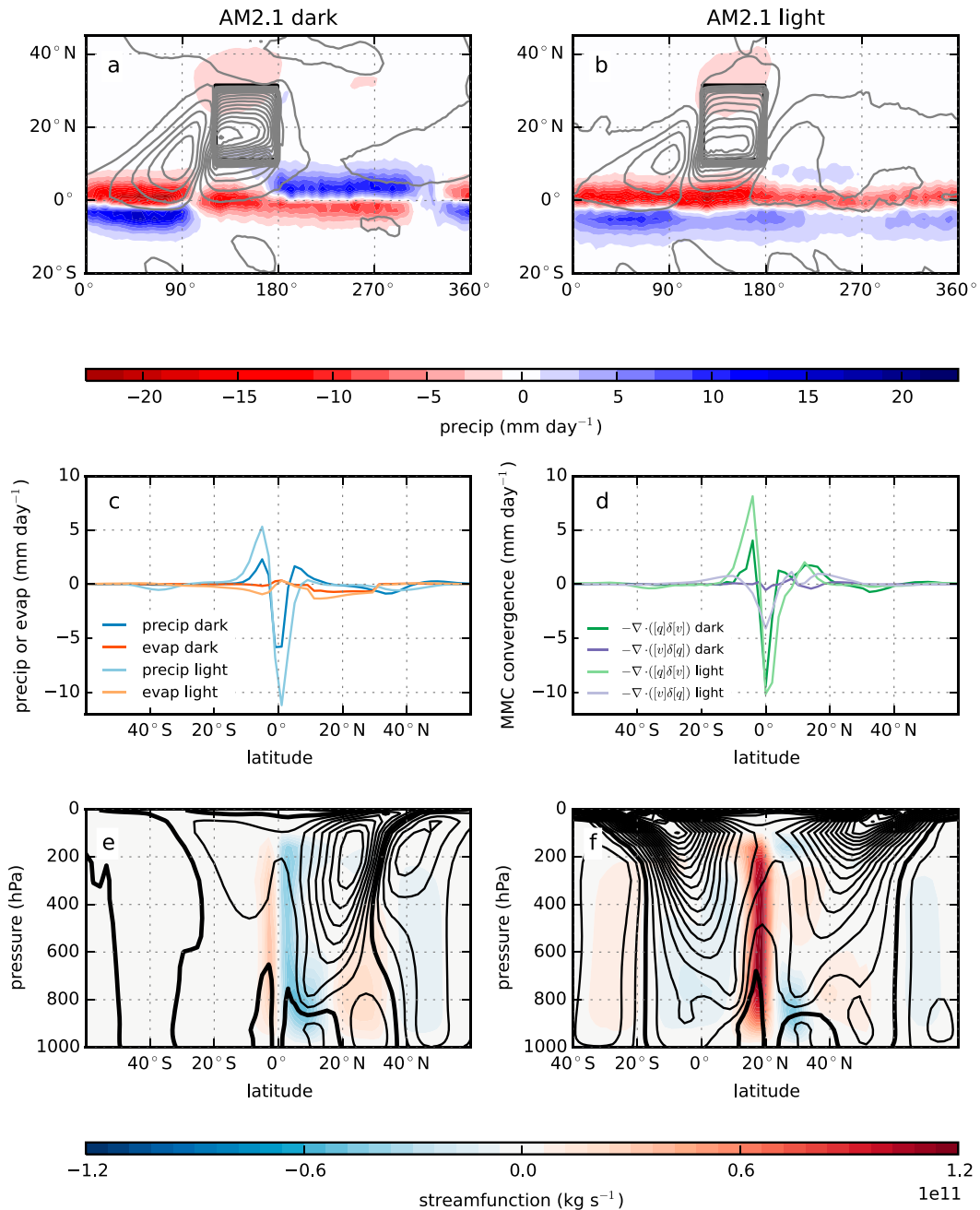


FIG. 7. As in Fig. 2, but for changes in the annual mean AM2.1 dark and light continent simulations. Note the larger range of the y axes in (c),(d) as compared to Figs. 2c,d.

increased subsidence creates stratocumulus clouds, which then maintain themselves. Their formation could be from subsidence due to a Rossby wave response from the monsoon region (as in Rodwell and Hoskins 1996) or from increased subsidence from the southward-shifted overturning circulation. Regardless, lower SST and subsidence from these clouds disfavor NH deep ascent in this region (Fig. 8a).

Over the southern part of the continent, LW radiation increases as a result of the increase of higher clouds from the weak monsoonlike circulation (Fig. 10e). Clear-sky OLR increases because of the hotter continent surface. As mentioned above, in the zonal mean, these regional TOA radiative changes together result in the NH having slightly more net radiation absorbed than the SH, mostly between the equator and 20°N (Fig. 9a).

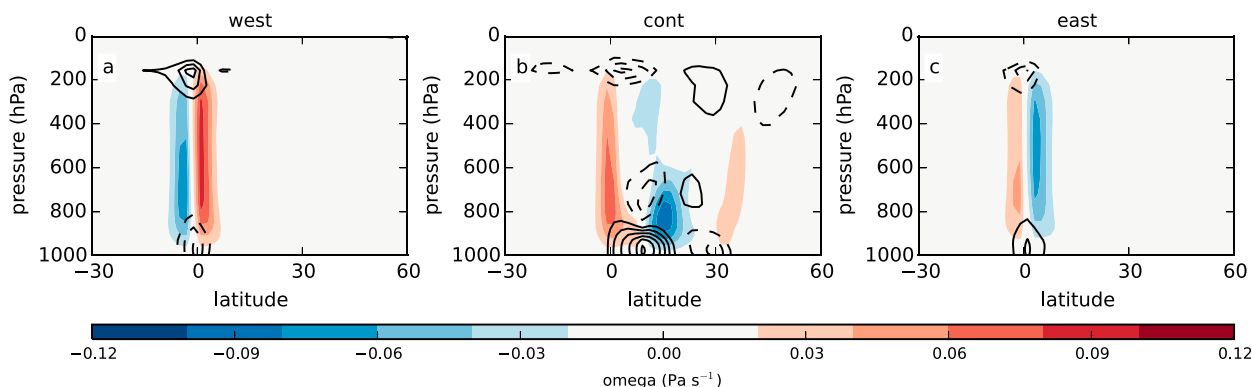


FIG. 8. Regional circulation changes in the dark AM2.1 simulation. (a) The change in zonal-mean meridional wind (contours) and pressure vertical velocity (shading) for the region to the west of the continent (330° – 120°) from the AM2.1 aquaplanet simulation. Also shown are the same quantities for (b) the continental region (120° – 180°) and (c) the region to the east of the continent (180° – 330°). Wind is contoured every 1 m s^{-1} , solid (dashed) contours indicate anomalous northward (southward) winds, and the zero contour is omitted.

An examination of individual APRP terms shows that SW changes most from changes in surface albedo, cloud fraction, or cloud scattering (not shown). Changes in cloud fraction and scattering contribute to the change in SW cloud forcing, with cloud fraction decrease most important over land and changes in scattering most important south of the continent; elsewhere cloud fraction and scattering share responsibility for changes. Unless surface albedo changes, the clear-sky SW radiation changes little; SW clear-sky radiation increases a little in the subtropics because of overcast sky surface albedo changes (cloud masking).

b. Continent simulations with varying albedo

Increasing the albedo of the continent creates a stronger interhemispheric difference in TOA net radiation

than in the dark simulation. In the light continent case where the land albedo is 0.30 (comparable to the albedo of Earth's deserts), the higher albedo decreases the NH absorbed SW radiation (Fig. 4c, light red line). In the zonal mean, this creates an anomalous Hadley circulation across the equator (Fig. 7f) that moves more energy to the NH, moves more moisture to the SH, and increases the precipitation in the SH relative to the NH, as compared with the dark simulation (Figs. 7a,b). The anomalous monsoonlike circulation over the continent is shallower than in the dark simulation likely because of decreased SW surface radiation absorption with the higher albedo. The NH jet decreases on the equatorward side but does not shift substantially (Fig. 7f).

The precipitation distribution in the light simulation has a different pattern from the dark simulation (Fig. 7b).

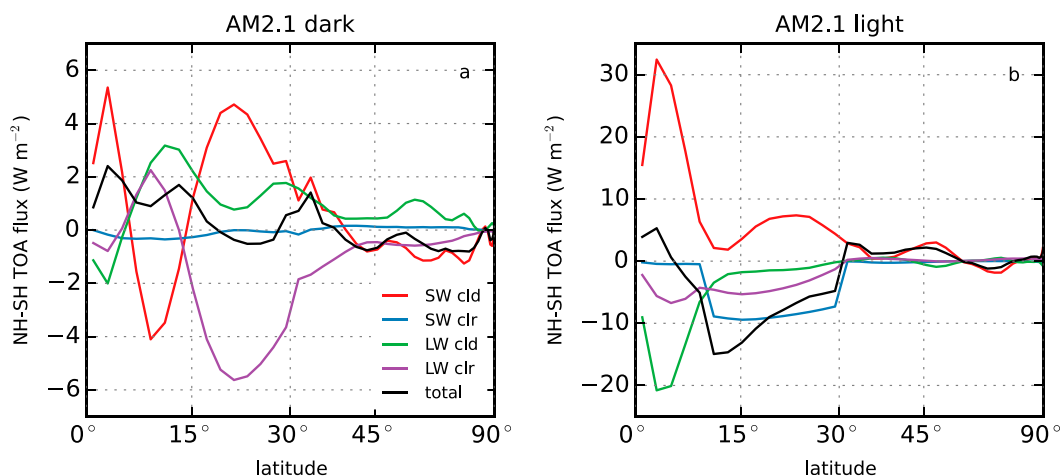


FIG. 9. Changes in the hemispheric difference of zonal-mean TOA radiation in (a) dark and (b) light albedo simulations compared to an AM2.1 aquaplanet simulation. NH–SH difference in total TOA radiation (black), SW cloudy-sky radiation (red), SW clear-sky radiation (blue), LW cloudy-sky radiation (green), and LW clear-sky radiation (purple) are shown. TOA LW and SW are defined to be positive when they add energy to the planet.

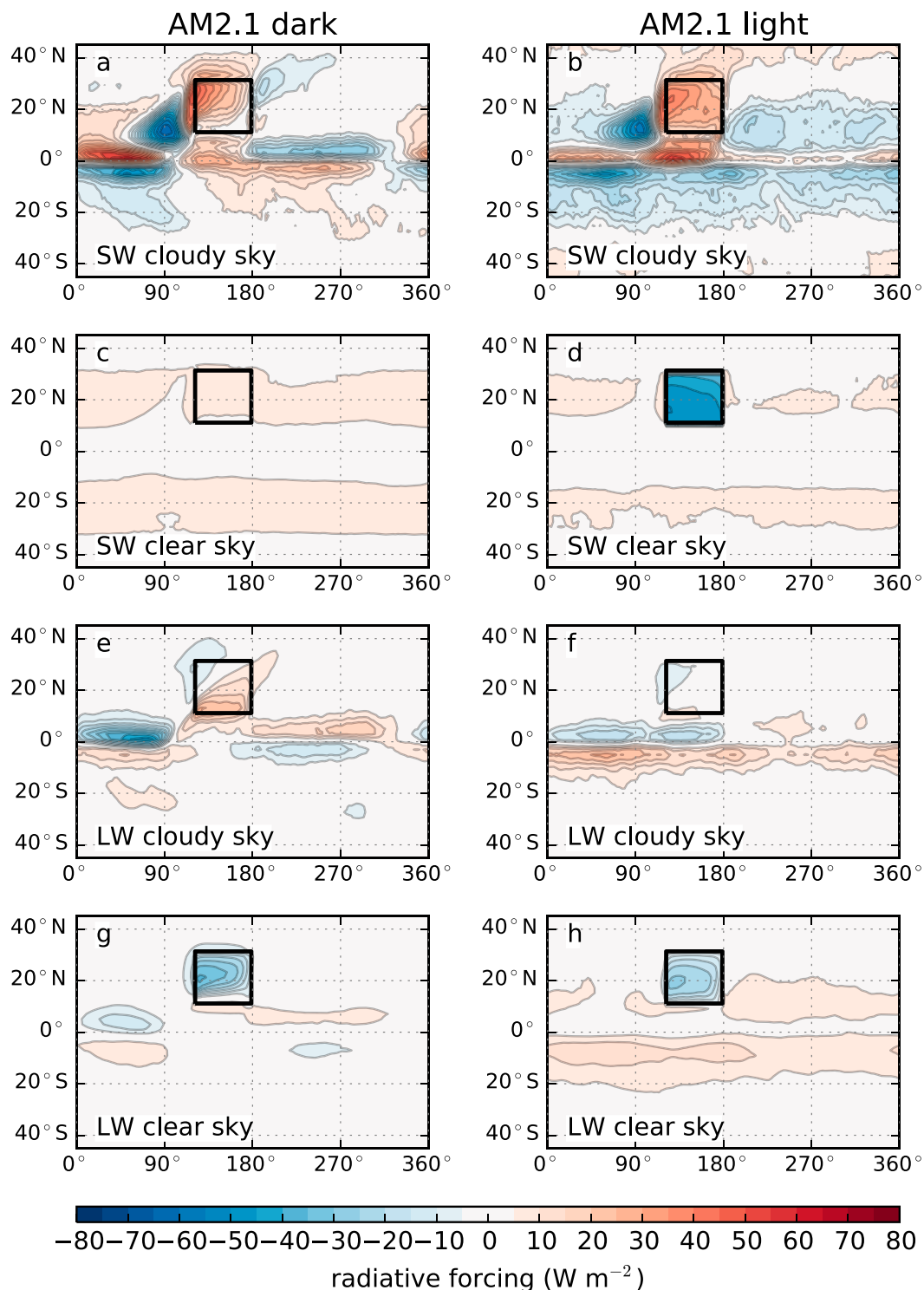


FIG. 10. Cloudy and clear sky decomposition of the TOA radiation budget for AM2.1 dark and light land albedo simulations. The anomalous change in SW cloudy-sky radiation from the aquaplanet simulation is shown for the (a) dark and (b) light albedo continent. Also shown are (c),(d) the SW clear-sky radiation change, (e),(f) the LW cloudy-sky radiation change, and (g),(h) the LW clear-sky radiation change. Changes in radiation that heat the planet are defined as positive.

The ITCZ shifts south of the equator everywhere in the light simulation, unlike in the dark simulation where it varied about the equator; the shift is still largest to the continent's west. Because the ITCZ shifts southward everywhere in the light simulation, the changes in SW and LW radiative forcing in the deep tropics are more zonally uniform than in the dark continent case (Figs. 9b and 10b,d,f,h). As in the dark simulation, the ITCZ shift determines the change in local radiative forcing because it moves moisture and deep clouds (Fig. 10). In the ITCZ region, the change in TOA SW cloud radiation is larger than the opposing change in the total TOA LW radiation. Our result that SW changes outweigh LW changes was also found in Kang et al. (2014) but differs from the simulations using other forcing types in AM2.1 where changes in total LW radiation were greater than the SW radiation in the ITCZ shift (see, e.g., Maroon et al. 2015; Woelfle et al. 2015). Cloud responses are likely model dependent; in the Community Atmosphere Model simulations from Cvijanovic and Chiang (2013), the LW radiation response was larger than the SW radiation response. Because of the SW radiation dominance in the ITCZ shift, the NH has greater net radiation absorbed than the SH in the deep tropics (Fig. 9b, black line).

The NH–SH difference in TOA radiation changes most in the subtropics, where the increased albedo has largely reduced the absorbed SW radiation over the NH continent (Fig. 10d). As in the dark simulation, clouds decrease over the dry continent, which increases the absorbed SW cloud forcing in that region. The hotter surface also increases the clear-sky OLR. Stratus clouds again form off the west coast of the continent, which decreases absorbed SW cloud radiation. In the zonal mean, these effects largely offset each other between 10° and 30°N, and the NH–SH net radiation difference is of the same sign and similar magnitude to the change in SW clear-sky radiation due to the change in surface albedo (Fig. 9b). Because other terms compensate, the change in clear-sky SW radiation from albedo largely determines which hemisphere receives more tropical precipitation (Fig. 6).

These results are similar for AM2.1 simulations with albedos higher than 0.06. The NH–SH difference in SW cloudy-sky radiation and LW total radiation compensate in the other AM2.1 simulations with varying land albedo (Figs. 6d,e). Except for the simulations with the highest and lowest albedo, all simulations show a similar response to the continent's west (Fig. 7b): the formation of stratocumulus clouds is a robust result that decreases the absorbed SW radiation in the NH relative to the SH, regardless of land albedo. These clouds also create an interhemispheric imbalance in TOA radiation that in isolation would amplify the southward ITCZ shift.

As albedo increases, the tropical rainfall distribution changes from a longitudinally varying structure (as in the dark simulation) into a zonally coherent southward ITCZ shift (as in the light simulation). The 0.2-albedo simulation shows this evolution between the dark and light simulations described above. The 0.2-albedo case has a southward shift to the continent's west that is similar to the dark simulation but a weak northward shift on the continent's east side. As the precipitation shifts change, the NH–SH difference in TOA net radiation follows the precipitation shifts (Figs. 7a,b). West of the continent, the NH–SH difference in TOA radiation does not change until an albedo of 0.6 is reached. East of the continent, the NH–SH difference in radiation changes sign with increasing albedo. With the brightest albedo, there is a uniform southward precipitation shift. The ITCZ is in the SH everywhere with no ascent over the continent.

5. Including the seasonal cycle in AM2.1 simulations

Next we examine the robustness of the precipitation shifts with a subtropical continent when the seasonal cycle is included in AM2.1. The aquaplanet control simulation has a broad equator-centered ITCZ with off-equatorial peaks that have a small amount of random asymmetry (Fig. 11a). The seasonal cycle is responsible for the peaks in precipitation on either side of the equator. Seasonally varying midlatitude storm tracks are also present (Fig. 12a). The annual mean overturning streamfunction and jets are weaker than in the annual mean insolation AM2.1 aquaplanet simulation (Fig. 13).

With a dark continent in a simulation with seasonal insolation, continental evaporation decreases (Fig. 11b, dark gray lines). In the annual mean, both peaks in tropical precipitation shift southward slightly (Figs. 11b,c). The ITCZ migrates across the equator faster with the continent (Fig. 12b). Compared to the aquaplanet simulation, the ITCZ in the dark simulation is farther south from October to March as it moves to the SH, while from May to August, the ITCZ is farther northward as it moves to the NH. Figures 11e,g show that precipitation is farther poleward in both JJA and DJF than in the aquaplanet simulation. This simulation has soil saturation and runoff, unlike the annual mean insolation simulations.

Changes in overturning streamfunction match the precipitation changes. Adding a dark continent causes a small annual mean circulation change in the form of a shallow monsoon circulation with ascent near 20°N (Fig. 14a). The subtropical continent strengthens the solstice-season winter hemisphere Hadley circulation

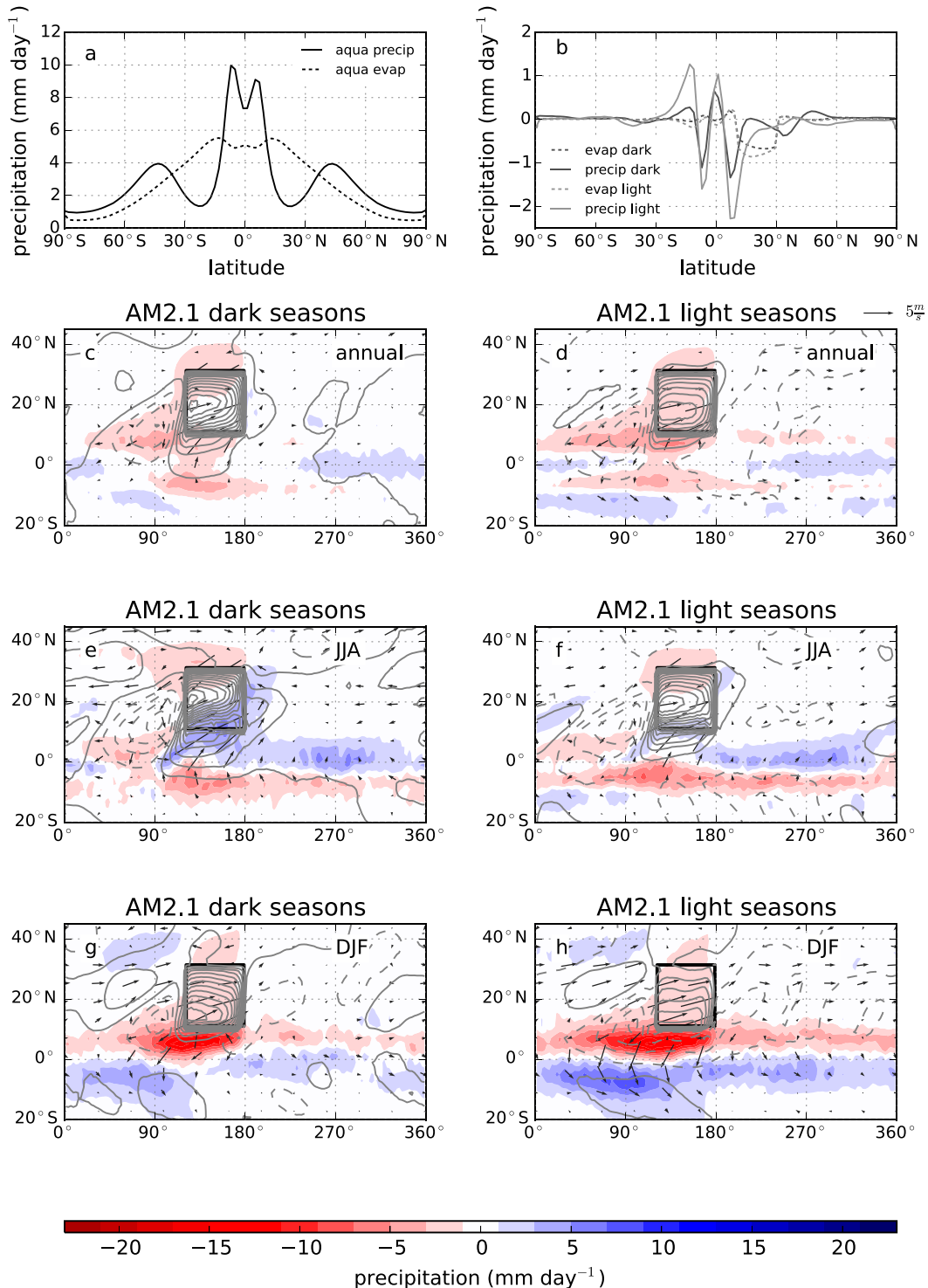


FIG. 11. Precipitation, evaporation, surface temperature, and 10-m wind changes in AM2.1 seasonal cycle simulations. (a) The aquaplanet zonal mean precipitation (solid lines) and evaporation (dashed lines). (b) The difference of the dark and light land albedo precipitation and evaporation from the aquaplanet. The difference in annual mean precipitation (shading), SST (contours), and 10-m wind (arrows) of the (c) dark and (d) light albedo simulations from the aquaplanet simulation. (e),(f) As in (c),(d), but for JJA. (g),(h) As in (c),(d), but for DJF. Contour intervals for SST are the same as in Figs. 2a and 7a.

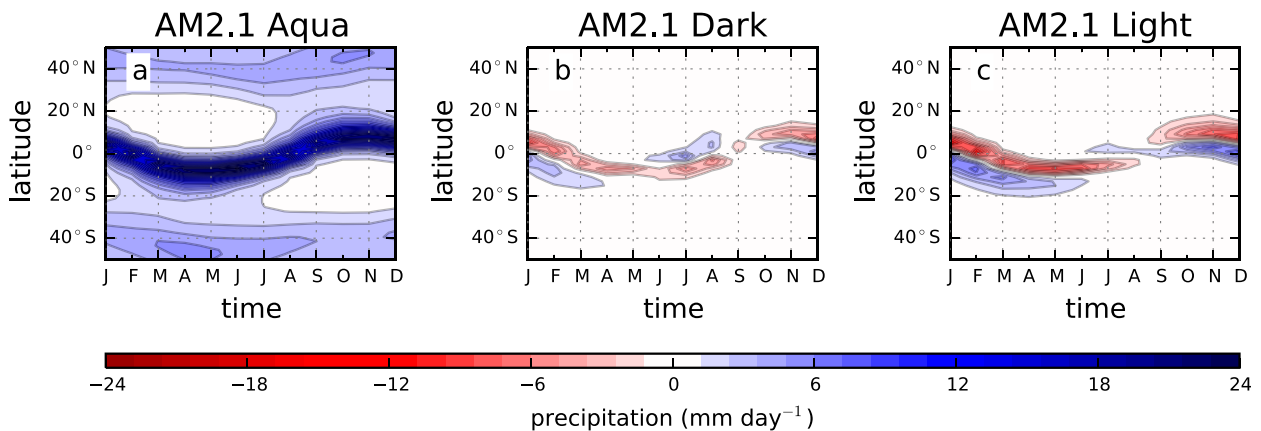


FIG. 12. (a) The seasonal cycle of precipitation in an AM2.1 aquaplanet simulation and the difference of (b) dark and (c) light land albedo simulations with a seasonal cycle from the aquaplanet.

from the aquaplanet (Figs. 14c,e). These results are similar to simulations in Cook (2003) where the presence of realistic continents doubles the strength of the winter hemisphere Hadley cells. In both JJA and DJF, anomalous southwesterly 10-m winds at the southwest corner of the continent decrease the trade winds. In JJA, this flow is strong enough to reverse the trade winds, resulting in a low-level westerly jet, reminiscent of the West African westerly jet (Grodsky et al. 2003; Pu and Cook 2012). This low-level jet is not present in the annual mean simulations.

In the dark simulation with seasons, annual mean SST increases south of the continent where annual mean precipitation also decreases, just as in the earlier dark simulation with annual mean insolation (Fig. 11c). Precipitation and SST increase together during JJA when the monsoonlike circulation is strongest (Fig. 11e). However, the DJF precipitation decrease is larger than the JJA increase and occurs alongside a modest SST increase near the continent (Fig. 11g); the changes in SST are not as important as the extra southward moisture transport due to the strengthened winter monsoon circulation. To the continent's west where low clouds form, SST and precipitation decrease together year-round. While the SST and precipitation changes are consistent in JJA and in the low cloud region, SST alone does not always diagnose the change in annual mean precipitation everywhere.

Although the addition of the continent causes large changes in SW cloudy-sky and LW clear-sky radiation over the continent, the hemispheric difference in TOA radiation is close to zero over the continent (Figs. 15a and 16a,g). The weak southward shift in precipitation is consistent with greater absorbed energy in the SH, but some of the precipitation change in this simulation is due to a decrease in evaporation.

Some aspects of the TOA radiation changes are similar to those in the annual mean insolation simulations (Fig. 10 vs Fig. 16). SW cloudy-sky radiation increases over the continent and decreases over the low cloud deck to the continent's west. The decrease in SW cloudy-sky radiation from increased low clouds is weaker than in the annual mean simulation. LW clear-sky radiation decreases over the continent because of greater OLR, as before. The ITCZ shifts are smaller in this simulation and the corresponding shifts in TOA radiation are also smaller. There is some hint of opposing changes in SW and LW cloudy-sky radiation, especially southwest of the continent.

With a higher albedo (0.3), precipitation shifts farther south, especially the SH ITCZ (Figs. 11b,d). The increase in albedo limits the amount of precipitation that reaches the continent. An anomalous Hadley circulation

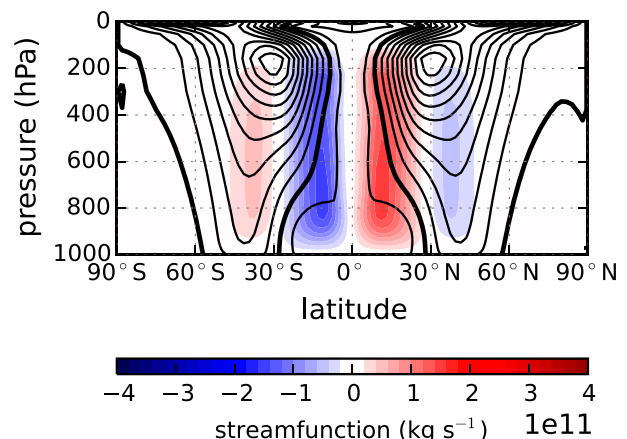


FIG. 13. Circulation in the AM2.1 aquaplanet simulation with seasonal cycle. Quantities and shading intervals are the same as in Figs. 1c,d.

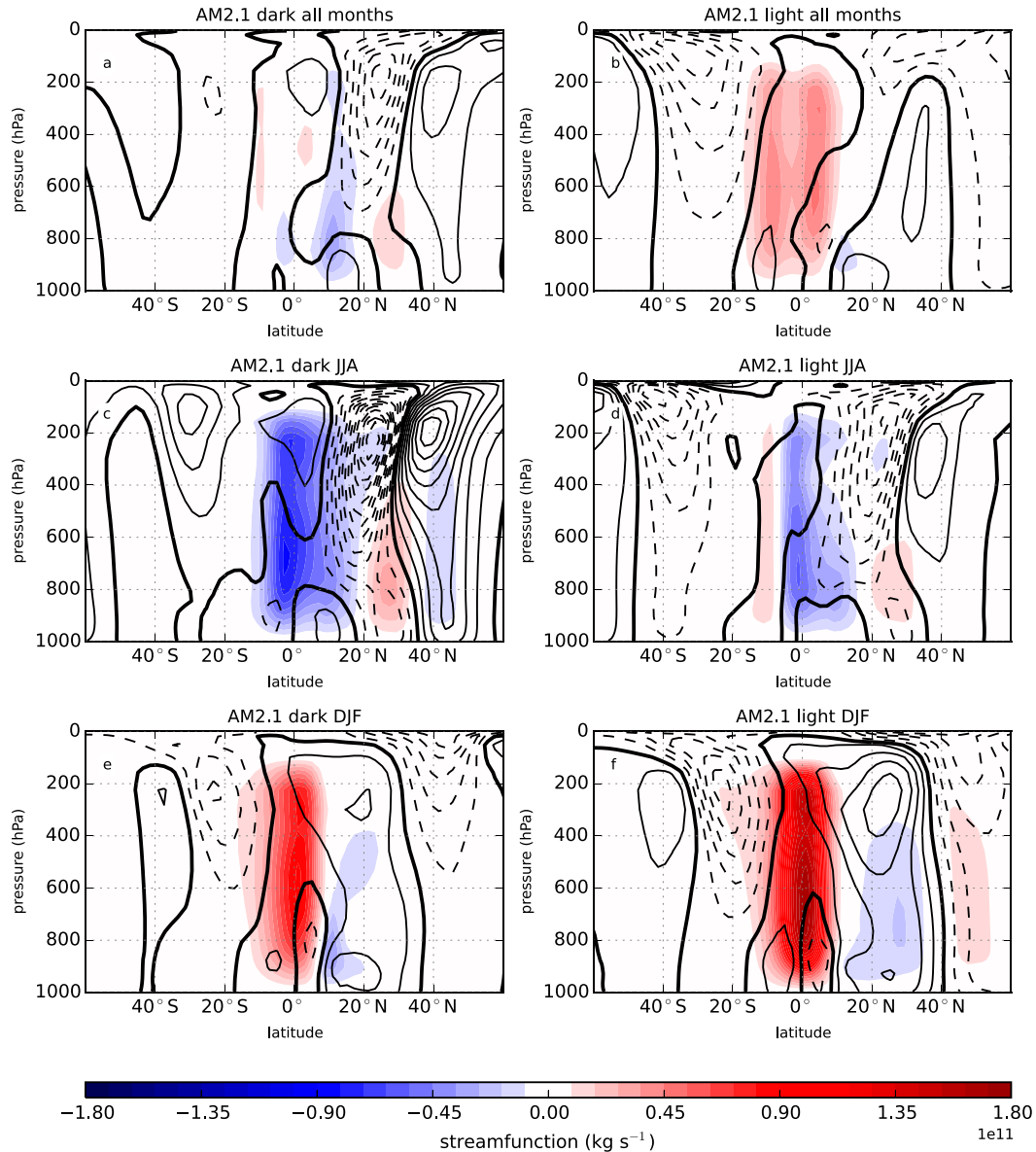


FIG. 14. Changes in streamfunction (shading) and zonal wind (contours) for (a) dark and (b) light continent simulations with a seasonal cycle as compared to the AM2.1 aquaplanet simulation with seasonal cycle. The annual mean differences are shown for the dark and light albedo simulations. (c),(d) As in (a),(b), but for JJA. (e),(f) As in (a),(b), but for DJF. Blue (red) shading denotes counterclockwise (clockwise) circulation. Wind is contoured every 1 m s^{-1} , with positive contours solid, negative contours dashed, and the zero-contour thickened.

forms across the equator with its upper branch moving mass and energy into the NH (Fig. 14b). The solstice-season precipitation and anomalous Hadley cells are still stronger than in the aquaplanet simulation (Figs. 11f,h and 14d,f). However, the asymmetry between JJA and DJF increases when compared to the dark albedo simulation. The amplified seasonal shift of the ITCZ into the SH now occurs from September through May and has increased in magnitude (Fig. 12c). The shift during JJA decreases. The winter hemisphere Hadley cells in

both solstice seasons are stronger than in the aquaplanet, but the DJF cell is stronger than the JJA cell in the light simulation. In addition, the addition of the light continent causes an SH jet shift and southward ITCZ shift in DJF, similar to results in Ceppi et al. (2013).

Annual mean SST south of the continent increases, while annual mean precipitation decreases in the light simulation (Fig. 11d). In contrast to the dark seasonal cycle simulation, JJA precipitation does not change while SST increases to the south of the continent

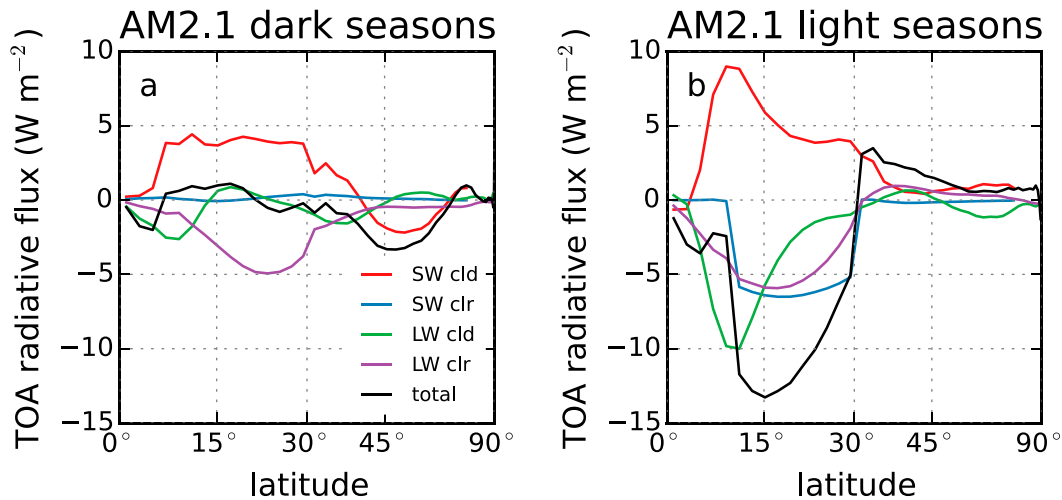


FIG. 15. Changes in the hemispheric difference of zonal-mean TOA radiation in (a) dark and (b) light albedo simulations with seasons compared to an AM2.1 aquaplanet simulation with seasons. Colored lines and quantities are the same as in Fig. 9.

(Fig. 11e vs Fig. 11f). The light simulation JJA anomalous Hadley cell is weaker than the dark simulation's, indicating less northward moisture transport to the continent, while the SST is higher because of its proximity to the continent. JJA precipitation also increases east of the continent, while SST there does not change. In DJF, precipitation and SST decrease together consistently. These results support the idea that SST changes alone do not always explain the changes in precipitation location.

The higher albedo leads to a larger NH–SH TOA radiation difference (Fig. 15b), just as in the annual mean insolation simulations. While SW cloudy-sky radiation increases over land (Fig. 16b), LW clear-sky radiation decreases over land when compared with the dark continent simulation (Fig. 16h), also like the annual mean insolation simulations (Fig. 10h). In addition, LW cloudy-sky radiation decreases in the NH tropics and increases in the SH from the larger southward ITCZ shift (Fig. 16f). LW cloudy-sky radiation also changes similarly in the annual mean simulation (Fig. 10f). As a result, the hemispheric difference in net radiation is larger than that from changes in surface albedo alone. The cloudy and clear sky changes amplify the NH energy deficit and the southward shift of the ITCZ. The details of the seasonal cycle simulation's radiation budget differ from those of the annual mean insolation simulations (e.g., larger SW cloud radiation changes outside the continent), but the addition of seasons does not change the qualitative results.

6. Summary and conclusions

The precipitation response to the addition of a subtropical continent has been studied in two AGCMs of

differing complexity. In GRaM, which lacks radiative feedbacks, the primary response to a subtropical continent is to decrease precipitation in the NH because of decreased evaporation over the dry continent. As the land albedo increases, a weak, anomalous Hadley circulation transports moisture to the SH, in addition to the evaporation-driven response.

The annual mean AM2.1 simulations have a zonally varying precipitation response, but the main result, that a bright continent shifts zonal mean tropical precipitation southward, is the same. Evaporation changes are relatively unimportant in the AM2.1 simulations; deep circulation changes are responsible for the altered precipitation distribution. The changes in clouds and water vapor amplify the Hadley circulation response. In the deep tropics, the ITCZ shift creates compensating clear and cloudy sky responses, with the SW radiation slightly dominating the balance; the cloud response would likely differ in other models. The surface albedo sets the hemispheric difference in net radiation because the total LW and SW cloud radiation changes compensate. As a result, the continent's albedo determines the location of greater precipitation. These simulations support Chou et al.'s (2001) result that high land albedo limits the northward extent of the monsoon and paleoclimate studies of the green Sahara that point to the importance of albedo–precipitation feedbacks (Kutzbach et al. 1996; Bonfils et al. 2001; Levis et al. 2004).

AM2.1 simulations with seasons share the main results in the annual mean simulations. The ITCZ shifts in the seasonal simulations are weaker, partially owing to the broader aquaplanet ITCZ. The changes in TOA radiation components are qualitatively similar. The

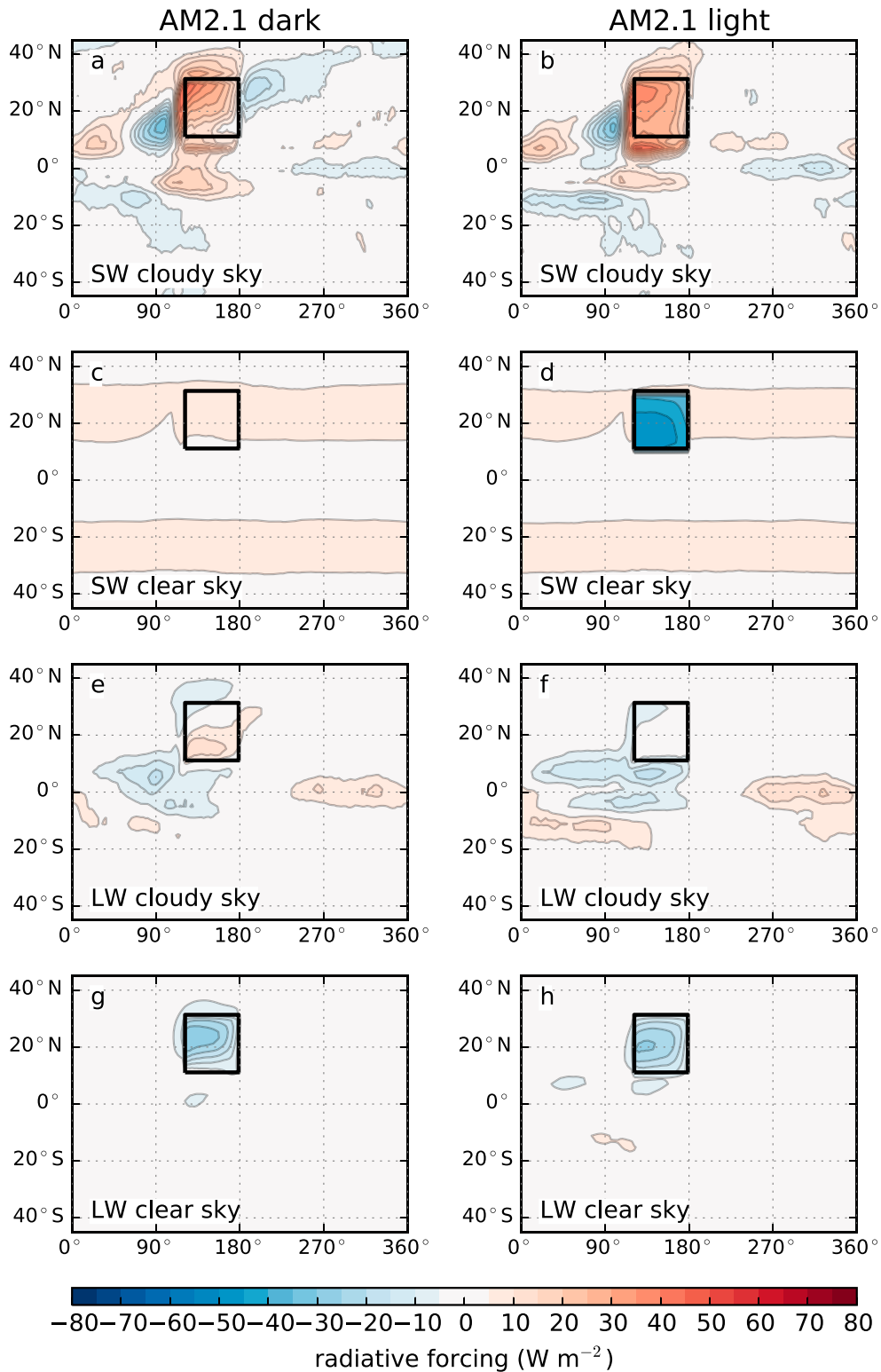


FIG. 16. As in Fig. 10, but for AM2.1 dark and light land albedo simulations with a seasonal cycle.

ITCZ shifts southward with increasing albedo, though the seasonal cycle changes many details of the radiation decomposition. The presence of a single continent strengthens the cross-equatorial Hadley cell during solstice seasons, as seen in Cook (2003). Although we do not include ocean heat transport, the results of Chou et al. (2001) and Clement (2006) indicate that surface fluxes are also important for the seasonal Hadley circulation.

Surface temperature alone does not dictate which hemisphere should have the greater precipitation. Rather, the hemispheric difference in TOA net radiation is more important because of its impact on the Hadley circulation. All GRaM and AM2.1 annual mean simulations with land have an NH with higher surface temperature, but some of these simulations also have an NH that was a net energetic sink (both GRaM simulations and the light AM2.1 simulation). When evaporation is included, the energetic perspective correctly predicts the hemisphere of greater precipitation. When examining tropical SST (which, based on the conclusions of a significant body of literature on tropical precipitation, should more directly control the ITCZ), tropical precipitation in the dark GRaM simulation was better predicted by TOA net radiation than by SST. The hemisphere with the continent is warmer in terms of land and ocean surface temperature but has less MSE.

Frierson et al. (2013) showed that without examining ocean heat transport, the Saharan energy sink should constrain the SH as the ITCZ location. Our continent with bright albedo shows this result as well, further indicating the importance of the ocean heat transport from the Atlantic meridional overturning circulation in the observed zonally averaged location of tropical precipitation. The regionally shifting ITCZ in our AM2.1 continent simulations should not be compared to observations; this steady response is not seen in the simulations with seasonally varying insolation. Rather, the relevant result is that the ITCZ shifts southward zonally because of the addition of a hot subtropical continent with a bright albedo. This result is robust to the addition of seasonal insolation.

The study of single continents in an AGCM examines the fundamental influence that land has on tropical precipitation, circulation, and radiation in isolation of other geographic features. Without other continents, this single continent setup could be used for climate model comparisons to study ocean–land–atmosphere interactions among models and how past albedo changes may have altered precipitation.

Acknowledgments. The authors wish to thank three anonymous reviewers for their constructive comments that improved this manuscript. EAM was supported by an

NDSEG fellowship and an NSF IGERT Program on Ocean Change traineeship. DMWF, EAM, and JS were supported by NSF Grants AGS-0846641, AGS-0936059, AGS-1359464, and PLR-1341497 and a UW Royalty Research Fund grant. SMK was supported by the Basic Science Research Program through the National Research Foundation of Korea (NRF) funded by the Ministry of Science, ICT and Future Planning (2013R1A1A3004589). JS was supported by AGS-1433551.

REFERENCES

- Anderson, J. L., and Coauthors, 2004: The new GFDL global atmosphere and land model AM2–LM2: Evaluation with prescribed SST simulations. *J. Climate*, **17**, 4089–4098, doi:10.1175/1520-0442(2004)017<4089:IOALMO>2.0.CO;2.
- Arbuszewski, J. A., P. B. deMenocal, C. Cléroux, L. Bradtmiller, and A. Mix, 2013: Meridional shifts of the Atlantic intertropical convergence zone since the Last Glacial Maximum. *Nat. Geosci.*, **6**, 959–962, doi:10.1038/ngeo1961.
- Ba, M. B., R. Frouin, S. E. Nicholson, and G. Dedieu, 2001: Satellite-derived surface radiation budget over the African continent. Part I: Estimation of downward solar irradiance and albedo. *J. Climate*, **14**, 45–58, doi:10.1175/1520-0442(2001)014<0045:SDSRBO>2.0.CO;2.
- Black, D. E., L. C. Peterson, J. T. Overpeck, A. Kaplan, M. N. Evans, and M. K. Kashgarian, 1999: Eight centuries of North Atlantic Ocean atmosphere variability. *Science*, **286**, 1709–1713, doi:10.1126/science.286.5445.1709.
- Bonfils, C., N. de Noblet-Ducoudré, P. Braconnot, and S. Joussaume, 2001: Hot desert albedo and climate change: Mid-Holocene monsoon in North Africa. *J. Climate*, **14**, 3724–3737, doi:10.1175/1520-0442(2001)014<3724:HDAACC>2.0.CO;2.
- Bordoni, S., and T. Schneider, 2008: Monsoons as eddy-mediated regime transitions of the tropical overturning circulation. *Nat. Geosci.*, **1**, 515–519, doi:10.1038/ngeo248.
- Broccoli, A. J., K. A. Dahl, and R. J. Stouffer, 2006: Response of the ITCZ to Northern Hemisphere cooling. *Geophys. Res. Lett.*, **33**, L01702, doi:10.1029/2005GL024546.
- Ceppi, P., Y.-T. Hwang, X. Liu, D. M. W. Frierson, and D. L. Hartmann, 2013: The relationship between the ITCZ and the Southern Hemispheric eddy-driven jet. *J. Geophys. Res. Atmos.*, **118**, 5136–5146, doi:10.1002/jgrd.50461.
- Chao, W. C., and B. Chen, 2001: The origin of monsoons. *J. Atmos. Sci.*, **58**, 3497–3507, doi:10.1175/1520-0469(2001)058<3497:TOOM>2.0.CO;2.
- Chiang, J. C. H., and C. M. Bitz, 2005: Influence of high latitude ice cover on the marine intertropical convergence zone. *Climate Dyn.*, **25**, 477–496, doi:10.1007/s00382-005-0040-5.
- , M. Biasutti, and D. S. Battisti, 2003: Sensitivity of the Atlantic intertropical convergence zone to Last Glacial Maximum boundary conditions. *Paleoceanography*, **18**, 1094, doi:10.1029/2003PA000916.
- Chou, C., and J. D. Neelin, 2001: Mechanisms limiting the southward extent of the South American summer monsoon. *Geophys. Res. Lett.*, **28**, 2433–2436, doi:10.1029/2000GL012138.
- , and —, 2003: Mechanisms limiting the northward extent of the northern summer monsoons over North America, Asia, and Africa. *J. Climate*, **16**, 406–425, doi:10.1175/1520-0442(2003)016<0406:MLTNEO>2.0.CO;2.

- , —, and H. Su, 2001: Ocean-atmosphere-land feedbacks in an idealized monsoon. *Quart. J. Roy. Meteor. Soc.*, **127**, 1869–1891, doi:10.1002/qj.49712757602.
- Clement, A. C., 2006: The role of the ocean in the seasonal cycle of the Hadley circulation. *J. Atmos. Sci.*, **63**, 3351–3365, doi:10.1175/JAS3811.1.
- Cook, K. H., 2003: Role of continents in driving the Hadley cells. *J. Atmos. Sci.*, **60**, 957–976, doi:10.1175/1520-0469(2003)060<0957:ROCIDT>2.0.CO;2.
- , and A. Gnanadesikan, 1991: Effects of saturated and dry land surfaces on the tropical circulation and precipitation in a general circulation model. *J. Climate*, **4**, 873–889, doi:10.1175/1520-0442(1991)004<0873:EOSADL>2.0.CO;2.
- Cvijanovic, I., and J. C. H. Chiang, 2013: Global energy budget changes to high latitude North Atlantic cooling and the tropical ITCZ response. *Climate Dyn.*, **40**, 1435–1452, doi:10.1007/s00382-012-1482-1.
- Delworth, T. L., and Coauthors, 2006: GFDL's CM2 global coupled climate models. Part I: Formulation and simulation characteristics. *J. Climate*, **19**, 643–674, doi:10.1175/JCLI3629.1.
- Dima, I. M., and J. M. Wallace, 2003: On the seasonality of the Hadley cell. *J. Atmos. Sci.*, **60**, 1522–1527, doi:10.1175/1520-0469(2003)060<1522:OTSOTH>2.0.CO;2.
- Emanuel, K. A., J. D. Neelin, and C. S. Bretherton, 1994: On large-scale circulations in convecting atmospheres. *Quart. J. Roy. Meteor. Soc.*, **120**, 1111–1143, doi:10.1002/qj.49712051902.
- Farneti, R., and G. K. Vallis, 2009: An Intermediate Complexity Climate Model (ICCMp1) based on the GFDL flexible modelling system. *Geosci. Model Dev.*, **2**, 73–88, doi:10.5194/gmd-2-73-2009.
- Frierson, D. M. W., 2007: The dynamics of idealized convection schemes and their effect on the zonally averaged tropical circulation. *J. Atmos. Sci.*, **64**, 1959–1976, doi:10.1175/JAS3935.1.
- , and Y.-T. Hwang, 2012: Extratropical influence on ITCZ shifts in slab ocean simulations of global warming. *J. Climate*, **25**, 720–733, doi:10.1175/JCLI-D-11-00116.1.
- , I. M. Held, and P. Zurita-Gotor, 2006: A gray-radiation aquaplanet moist GCM. Part I: Static stability and eddy scale. *J. Atmos. Sci.*, **63**, 2548–2566, doi:10.1175/JAS3753.1.
- , and Coauthors, 2013: Contribution of ocean overturning circulation to tropical rainfall peak in the Northern Hemisphere. *Nat. Geosci.*, **6**, 940–944, doi:10.1038/ngeo1987.
- Fučkar, N. S., S.-P. Xie, R. Farneti, E. A. Maroon, and D. M. W. Frierson, 2013: Influence of the extratropical ocean circulation on the intertropical convergence zone in an idealized coupled general circulation model. *J. Climate*, **26**, 4612–4629, doi:10.1175/JCLI-D-12-00294.1.
- Gadgil, S., 2003: The Indian monsoon and its variability. *Annu. Rev. Earth Planet. Sci.*, **31**, 429–467, doi:10.1146/annurev.earth.31.100901.141251.
- , P. V. Joseph, and N. V. Joshi, 1984: Ocean-atmosphere coupling over monsoon regions. *Nature*, **312**, 141–143, doi:10.1038/312141a0.
- Gill, A. E., 1980: Some simple solutions for heat-induced tropical circulation. *Quart. J. Roy. Meteor. Soc.*, **106**, 447–462, doi:10.1002/qj.49710644905.
- Grodsky, S. A., J. A. Carton, and S. Nigam, 2003: Near surface westerly wind jet in the Atlantic ITCZ. *Geophys. Res. Lett.*, **30**, 2009, doi:10.1029/2003GL017867.
- Haug, G. H., K. A. Hughen, D. M. Sigman, L. C. Peterson, and U. Rohl, 2001: Southward migration of the intertropical convergence zone through the Holocene. *Science*, **293**, 1304–1308, doi:10.1126/science.1059725.
- Held, I. M., and A. Y. Hou, 1980: Nonlinear axially symmetric circulations in a nearly inviscid atmosphere. *J. Atmos. Sci.*, **37**, 515–533, doi:10.1175/1520-0469(1980)037<0515:NASCIA>2.0.CO;2.
- Hoskins, B., and M. Rodwell, 1995: A model of the Asian summer monsoon. Part I: The global scale. *J. Atmos. Sci.*, **52**, 1329–1340, doi:10.1175/1520-0469(1995)052<1329:AMOTAS>2.0.CO;2.
- Hwang, Y.-T., D. M. W. Frierson, and S. M. Kang, 2013: Anthropogenic sulfate aerosol and the southward shift of tropical precipitation in the late 20th century. *Geophys. Res. Lett.*, **40**, 2845–2850, doi:10.1002/grl.50502.
- Kang, S. M., and I. M. Held, 2012: Tropical precipitation, SSTs and the surface energy budget: A zonally symmetric perspective. *Climate Dyn.*, **38**, 1917–1924, doi:10.1007/s00382-011-1048-7.
- , —, D. M. W. Frierson, and M. Zhao, 2008: The response of the ITCZ to extratropical thermal forcing: Idealized slab ocean experiments with a GCM. *J. Climate*, **21**, 3521–3532, doi:10.1175/2007JCLI2146.1.
- , D. M. W. Frierson, and I. M. Held, 2009: The tropical response to extratropical thermal forcing in an idealized GCM: The importance of radiative feedbacks and convective parameterization. *J. Atmos. Sci.*, **66**, 2812–2827, doi:10.1175/2009JAS2924.1.
- , I. M. Held, and S.-P. Xie, 2014: Contrasting the tropical responses to zonally asymmetric extratropical and tropical thermal forcing. *Climate Dyn.*, **42**, 2033–2043, doi:10.1007/s00382-013-1863-0.
- , B.-M. Kim, D. M. W. Frierson, S.-J. Jeong, J. Seo, and Y. Chae, 2015a: Seasonal dependence of the effect of Arctic greening on tropical precipitation. *J. Climate*, **28**, 6086–6095, doi:10.1175/JCLI-D-15-0079.1.
- , R. Seager, D. M. W. Frierson, and X. Liu, 2015b: Croll revisited: Why is the Northern Hemisphere warmer than the Southern Hemisphere? *Climate Dyn.*, **44**, 1457–1472, doi:10.1007/s00382-014-2147-z.
- Karnauskas, K. B., and C. C. Ummerhofer, 2014: On the dynamics of the Hadley circulation and subtropical drying. *Climate Dyn.*, **42**, 2259–2269, doi:10.1007/s00382-014-2129-1.
- Koutavas, A., and J. Lynch-Stieglitz, 2003: Glacial–interglacial dynamics of the eastern equatorial Pacific cold tongue intertropical convergence zone system reconstructed from oxygen isotope records. *Paleoceanography*, **18**, 1089, doi:10.1029/2003PA000894.
- Kutzbach, J., G. Bonan, J. Foley, and S. P. Harrison, 1996: Vegetation and soil feedbacks on the response of the African monsoon to orbital forcing in the early to middle Holocene. *Nature*, **384**, 623–626, doi:10.1038/384623a0.
- Levis, S., G. B. Bonan, and C. Bonfils, 2004: Soil feedback drives the mid-Holocene North African monsoon northward in fully coupled CCSM2 simulations with a dynamic vegetation model. *Climate Dyn.*, **23**, 791–802, doi:10.1007/s00382-004-0477-y.
- L'Heveder, B., F. Codron, and M. Ghil, 2015: Impact of anomalous northward ocean heat transport on global climate in a slab ocean setting. *J. Climate*, **28**, 2650–2664, doi:10.1175/JCLI-D-14-00377.1.
- Lindzen, R. S., and S. Nigam, 1987: On the role of sea surface temperature gradients in forcing low-level winds and convergence in the tropics. *J. Atmos. Sci.*, **44**, 2418–2436, doi:10.1175/1520-0469(1987)044<2418:OTROSS>2.0.CO;2.
- , and A. V. Hou, 1988: Hadley circulations for zonally averaged heating centered off the equator. *J. Atmos. Sci.*, **45**, 2416–2427, doi:10.1175/1520-0469(1988)045<2416:HCFZAH>2.0.CO;2.
- Manabe, S., 1969: Climate and the ocean circulation: The atmospheric circulation and the hydrology of the earth's surface. *Mon. Wea.*

- Rev.*, **97**, 739–773, doi:10.1175/1520-0493(1969)097<0739:CATOC>2.3.CO;2.
- Maroon, E. A., D. M. W. Frierson, and D. S. Battisti, 2015: The tropical precipitation response to Andes topography and ocean heat fluxes in an aquaplanet model. *J. Climate*, **28**, 381–398, doi:10.1175/JCLI-D-14-00188.1.
- Marshall, J., A. Donohoe, D. Ferreira, and D. McGee, 2013: The ocean's role in setting the mean position of the inter-tropical convergence zone. *Climate Dyn.*, **42**, 1967–1979, doi:10.1007/s00382-013-1767-z.
- Milly, P. C. D., and A. B. Shmakin, 2002: Global modeling of land water and energy balances. Part I: The Land Dynamics (LaD) model. *J. Hydrometeorol.*, **3**, 283–299, doi:10.1175/1525-7541(2002)003<0283:GMOLWA>2.0.CO;2.
- Moorthi, S., and M. J. Suarez, 1992: Relaxed Arakawa-Schubert. A parameterization of moist convection for general circulation models. *Mon. Wea. Rev.*, **120**, 978–1002, doi:10.1175/1520-0493(1992)120<0978:RASAP0>2.0.CO;2.
- Peixoto, J. P., and A. H. Oort, 1992: *Physics of Climate*. American Institute of Physics, 520 pp.
- Plumb, R., and A. Hou, 1992: The response of a zonally symmetric atmosphere to subtropical forcing: Threshold behavior. *J. Atmos. Sci.*, **49**, 1790–1799, doi:10.1175/1520-0469(1992)049<1790:TROAZS>2.0.CO;2.
- Privé, N. C., and R. A. Plumb, 2007a: Monsoon dynamics with interactive forcing. Part I: Axisymmetric studies. *J. Atmos. Sci.*, **64**, 1417–1430, doi:10.1175/JAS3916.1.
- , and —, 2007b: Monsoon dynamics with interactive forcing. Part II: Impact of eddies and asymmetric geometries. *J. Atmos. Sci.*, **64**, 1431–1442, doi:10.1175/JAS3917.1.
- Pu, B., and K. H. Cook, 2012: Role of the West African westerly jet in Sahel rainfall variation. *J. Climate*, **25**, 2880–2896, doi:10.1175/JCLI-D-11-00394.1.
- Ridley, H. E., and Coauthors, 2015: Aerosol forcing of the position of the intertropical convergence zone since AD 1550. *Nat. Geosci.*, **8**, 195–200, doi:10.1038/ngeo2353.
- Rodwell, M., and B. Hoskins, 1996: Monsoons and the dynamics of deserts. *Quart. J. Roy. Meteor. Soc.*, **122**, 1385–1404, doi:10.1002/qj.49712253408.
- Rotstayn, L. D., B. F. Ryan, and J. E. Penner, 2000: Precipitation changes in a GCM resulting from the indirect effects of anthropogenic aerosols. *Geophys. Res. Lett.*, **27**, 3045–3048, doi:10.1029/2000GL011737.
- Scheff, J., 2014: Understanding the responses of precipitation, evaporative demand, and terrestrial water availability to planetary temperature in climate models. Ph.D. dissertation, University of Washington, 199 pp. [Available online at <http://www.ideo.columbia.edu/~jscheff/JacobScheffUWDissertation.pdf>.]
- Seo, J., S. M. Kang, and D. M. W. Frierson, 2014: Sensitivity of intertropical convergence zone movement to the latitudinal position of thermal forcing. *J. Climate*, **27**, 3035–3042, doi:10.1175/JCLI-D-13-00691.1.
- Shi, X., and D. R. Durran, 2014: The response of orographic precipitation over idealized midlatitude mountains due to global increases in CO₂. *J. Climate*, **27**, 3938–3956, doi:10.1175/JCLI-D-13-00460.1.
- Sud, Y. C., G. K. Walker, and K.-M. Lau, 1999: Mechanisms regulating sea-surface temperatures and deep convection in the tropics. *Geophys. Res. Lett.*, **26**, 1019–1022, doi:10.1029/1999GL900197.
- Taylor, K. E., M. Crucifix, P. Braconnot, C. D. Hewitt, C. Doutriaux, A. J. Broccoli, J. F. B. Mitchell, and M. J. Webb, 2007: Estimating shortwave radiative forcing and response in climate models. *J. Climate*, **20**, 2530–2543, doi:10.1175/JCLI4143.1.
- Woelfle, M. D., C. S. Bretherton, and D. M. W. Frierson, 2015: Time scales of response to antisymmetric surface fluxes in an aquaplanet GCM. *Geophys. Res. Lett.*, **42**, 2555–2562, doi:10.1002/2015GL063372.
- Xie, S.-P., 2005: The shape of continents, air-sea interaction, and the rising branch of the Hadley circulation. *The Hadley Circulation: Past, Present and Future*, H. F. Diaz and R. S. Bradley, Eds., Springer, 121–152, doi:10.1007/978-1-4020-2944-8_5.
- Yoshimori, M., and A. J. Broccoli, 2008: Equilibrium response of an atmosphere–mixed layer ocean model to different radiative forcing agents: Global and zonal mean response. *J. Climate*, **21**, 4399–4423, doi:10.1175/2008JCLI2172.1.
- , and —, 2009: On the link between Hadley circulation changes and radiative feedback process. *Geophys. Res. Lett.*, **36**, L20703, doi:10.1029/2009GL040488.
- Zhang, C., 1993: Large-scale variability of atmospheric deep convection in relation to sea surface temperature in the tropics. *J. Climate*, **6**, 1898–1913, doi:10.1175/1520-0442(1993)006<1898:LSVOAD>2.0.CO;2.
- Zhang, R., and T. L. Delworth, 2005: Simulated tropical response to a substantial weakening of the Atlantic thermohaline circulation. *J. Climate*, **18**, 1853–1860, doi:10.1175/JCLI3460.1.